. FINAL REPORT

MEASUREMENT TECHNIQUES AND INSTRUMENTS SUITABLE FOR LIFE-PREDICTION TESTING OF PHOTOVOLTAIC ARRAYS

to

JET PROPULSION LABORATORY
CALIFORNIA INSTITUTE OF TECHNOLOGY

for the

ENCAPSULATION TASK OF THE
LOW-COST SOLAR ARRAY PROJECT

March 31, 1979

G. T. Noel, V. E. Wood, V. D. McGinniss, J. A. Hassell,
N. A. Richard, G. B. Gaines, and D. C. Carmichael

BATTELLE
Columbus Laboratories ·
505 King Avenue
Columbus, Ohio 43201

FINAL REPORT

MEASUREMENT TECHNIQUES AND INSTRUMENTS SUITABLE FOR LIFE-PREDICTION TESTING OF PHOTOVOLTAIC ARRAYS

to

JET PROPULSION LABORATORY
CALIFORNIA INSTITUTE OF TECHNOLOGY

for the

ENCAPSULATION TASK OF THE
LOW-COST SOLAR ARRAY PROJECT

March 31, 1979

G T. Noel, V E Wood, V D. McGinniss, J A Hassell,
N. A Richard, G B. Gaines, and D C Carmichael

BATTELLE
Columbus Laboratories
505 King Avenue
Columbus, Ohio 43201

MEASUREMENT TECHNIQUES AND INSTRUMENTS SUITABLE FOR LIFE-PREDICTION TESTING OF PHOTOVOLTAIC ARRAYS

ABSTRACT

The validation of a 20-year service life for low-cost photovoltaic arrays is a critical requirement in the Low-Cost Solar Array (LSA) Project that is being conducted by the Jet Propulsion Laboratory for the Department of Energy. Of necessity, this validation must be accomplished through accelerated life-prediction tests. A methodology for such tests has been developed in a preceding study at Battelle for the LSA Project Remaining needs before such tests are carried out are the identification, assessment, and experimental evaluation of diagnostic techniques and instruments that make it possible to measure failure-related degradative property changes over a short time period with sufficient precision to allow the prediction of service life exceeding 20 years.

A two-phase study has been conducted addressing these needs. Phase I, the results of which were discussed in the interim report on this study, accomplished the initial identification and assessment of all known measurement techniques and instruments that might be used in these life-prediction tests and included recommendations on their use. The results and recommended techniques from the Phase I investigation are summarized in the Appendix of this report.

Phase II of the study, covered in this report, consisted of experimental evaluations of three techniques selected from those recommended as a result of the Phase I findings. The three techniques evaluated were specular and nonspecular optical reflectometry, chemiluminescence measurements, and electrical current noise measurements.

The optical reflectance experiments included reflection and imaging of an expanded beam, point-by-point reflectometry, double-exposure holographic interferometry, imaging of scattered light by spatial filtering of a reflected coherent beam, and measurement of light scattering from a tangential beam propagating parallel to the cell surface. The principal focus of these experiments was on early detection and characterization of interface degradation, particularly delamination

The expanded beam technique was successful in detecting small delaminations (<1mm) between the adhesive layer and the plastic cover in encapsulation structures involving an acrylite cover and Scotchweld adhesive. Different illuminating wavelengths may be required to yield high contrast in modules of different composition.

The point-by-point technique yielded more detailed information on delaminated regions than the expanded beam technique, including the identification of potential incipient delamination regions A more sophisticated measurement system could allow quantitative assessments of the shape of the delaminated adhesive surface.

Development and automation of the technique to a level to allow a rapid statistical survey of photovoltaic modules is essential to the successful use of this approach.

The holographic interferometry technique was briefly explored and, while it did reveal some, but not all, delaminations and defects in a test sample, considerable development is necessary to make this technique suitable for widespread use.

The tangential beam technique is the most promising of the light-scattering techniques. This technique was successful in locating all significant defects and delaminations in the test sample down to a size of about 50 mm. If a means for injecting the tangential beam into the module without compromising the integrity of the encapsulation system can be provided, this appears to be potentially the most useful of all of the optical reflectance techniques explored

The chemiluminescence experiments were aimed at establishing the sensitivity of this technique as a tool for the early detection and quantification of UV-induced degradative changes in polymeric materials   The initial experiments were performed with high-purity PMMA films in order to establish viability with simple systems   The technique was found to be very sensitive in detecting first-order-decay emissions induced by UV illumination in the presence of oxygen   It is recommended that future studies involve correlation of chemiluminescence measurements with other sensitive techniques in order to establish a basis for long-term characterization of degradative changes in polymeric materials. Equipment modifications and developments that would enhance the effectiveness of the technique for this specific application are also recommended.

The measurement of electrical current noise, also known as 1/f noise, in photovoltaic devices was investigated as a means of evaluating series resistance changes due to corrosion or partial debonding of contact metallization. The noise characteristics of cells with stress-sensitive contacts were measured, including current dependence and spectral distribution. Series-resistance values were determined from I–V characteristics of the cells to assess correlations with noise measurements   In low-cost solar cell designs of the type tested in this evaluation, the magnitude of other types of low-frequency noise is significant with respect to the apparent 1/f noise levels. This made it difficult to distinguish the 1/f noise associated with contact degradation and also obscured any correlation with cell series resistance. Exposure of the cells to high humidity did, however, produce significant increases in the cells' noise output, although these changes did not correlate with apparent changes in cell series resistance. Further experiments are recommended to determine if the observed changes in noise generation can be correlated with other degradation modes and to establish the noise characteristics of other types of cells.

ACKNOWLEDGMENTS

TABLE OF CONTENTS

LIST OF TABLES

LIST OF FIGURES

LIST OF FIGURES
(Continued)

LIST OF FIGURES
(Continued)

SUMMARY

To aid in meeting the need for establishing reliable tests for characterizing the response with time of present and future encapsulated photovoltaic modules, a two-phase study was conducted to identify specific measurement requirements as well as applicable or potentially applicable measurement techniques for satisfying those requirements. Instruments suitable for these applications must provide high degrees of sensitivity and precision in order to establish confidence in conclusions drawn regarding the projected performance and operational life of alternative designs and materials

Phase I of the study reviewed relevant degradation modes and mechanisms, including contributing environmental stresses, and identified and recommended all techniques and instruments judged suitable for characterizing specific types and classes of degradation modes. One category of techniques identified and recommended included techniques which required some further experimental evaluation and/or developmental work in order to establish their applicability and sensitivity precision. This category of recommendations formed the basis for the Phase II evaluations

In Phase II, three techniques requiring such experimental evaluation were selected from those recommended in the Phase I study for a preliminary experimental evaluation. The techniques were selected on the basis of their potential advantage in sensitivity or in on-site applicability. Specular and nonspecular optical reflectance measurements were chosen because of their potential for on-site use in studying delamination, and other interface flaws and degradation modes. Chemiluminescence measurements were chosen for evaluating UV-radiation-induced degradative changes in polymers because they offer a high degree of sensitivity and precision in characterizing such changes. Electrical noise measurements were chosen for evaluating cell series-resistance changes associated with contact corrosion and/or debonding because of the inadequacy of conventional techniques and their potential adaptability to on-site use.

Optical Reflectance Experiments

The optical reflectance experiments focused on early detection and evaluation of delamination and its precursors Among the delaminative characteristics that might conceivably be quantified by optical methods are:

(1) Number of delaminations per unit area

(2) Average size of delaminations

(3) Areal distribution of delaminations according to size

(4) Shape of delaminations (circular, elliptical, irregular, etc.)

(5) Location of delaminations

(6) Degree of separation of delaminations

(7) Transverse cross section of delaminations

(8) Presence of material (water, gases, etc.) within delaminations

Specific optical reflectance experiments conducted include.

    (1) Overall reflection and imaging of an expanded coherent beam

    (2) Point–by–point reflectometry

    (3) Double–exposure holographic interferometry-

    (4) Imaging of scattered light by spatial filtering of a reflected coherent beam

    (5) Light scattering from a tangential beam propagating parallel to the cell surface.

Samples of cells encapsulated in several different ways were used in these experiments, including some modules removed from the Mead, Nebraska installation.

The specular reflectance studies (expanded beam and point–by–point) were successful in revealing a number of defect features in the test samples that would not have been immediately obvious with standard visual examination techniques   Derivation of quantitative information on, for example, the size and shape of delaminations was not possible for the experimental arrangement used, however, modifications that would permit this type of analysis are suggested.

Double exposure holography was only partially successful in detecting delaminations and some experimental difficulties were identified. Modifications that could improve the effectiveness of this technique are also identified.

Of the light–scattering techniques investigated, the tangential propagation of a coherent beam along an interface appears to be the most sensitive and potentially useful. The primary barrier to its use in the field will be injecting the beam at the desired interface without compromising the integrity of the module

Chemiluminescence Experiments

Chemiluminescence experiments were performed using high–purity polymethylmethacrylate films as test samples   The samples were exposed to ultraviolet radiation from a mercury light source under a controlled atmosphere of either air or dry nitrogen, and the magnitude and decay of the resulting chemiluminescence curve was evaluated. A series of filters was used to establish the sensitizing wavelength for the process which causes the observed chemiluminescence   The observable first–order–decay emissions are oxygen sensitive in that the initial chemiluminescence readings are somewhat higher in intensity under nitrogen than under oxygen. The absorption of ultraviolet radiation apparently causes polymer long–range–order or polymer–structure modifications, which give rise to the emissions   For life–prediction studies on photovoltaic modules, it is desirable to perform additional studies beyond the scope of this evaluation, including spectral analysis of the emitted light, and to establish correlations with other techniques such as ESR, GPC, etc.

Electrical Noise Measurements

Electrical current noise (l/f noise) has been found to be sensitive to the quality of electrical contacts on semiconductor devices. Measurements of the current noise characteristics of photovoltaic devices were made to establish the applicability of this type of measurement for characterizing degradative changes in the contact metallization of these devices. The cells used in these experiments were low–cost–process type cells with screen printed contact metallization, chosen because they had previously exhibited significant increases in series resistance upon exposure to high–humidity and thermal–cycling stresses. Both the current density dependence and the spectral distribution of low–frequency noise were investigated to determine if l/f noise might be dominant in this frequency range in photovoltaic cells. Comparisons of cell series resistance, and of changes in series resistance due to humidity and thermal stress, with measured noise values were also made to determine sensitivity and correlations The noise power was found to vary somewhat more slowly with current density than the I^2 dependence anticipated for current densities in the 0–25 mA/cm^2 range. At higher current densities (25–45 mA/cm^2) the variation was of higher order than I^2 (I^7 or higher in some cases) In addition, the noise characteristics of the cells did not exhibit significant frequency dependence approaching l/f type behavior except at very low frequencies (0–2 Hz). Current instabilities indicative of burst noise were also observed in many of the devices tested at moderate to high current densities.

No positive correlation between series–resistance values (and stress–induced changes in series resistance by high humidity) and measured noise characteristics of the cells used in these experiments was found However, high–humidity stressing did produce significant changes in the low–frequency noise of the devices. The results tend to indicate that noise sources other than those associated with classical l/f behavior may be significant in these devices. These noise sources would include generation–recombination noise and burst or "pop–corn" noise associated with device surface conditions. High–humidity stressing does produce significant changes in cell noise characteristics Whether these changes correlate with other types of degradation mechanisms in cells has not been established. The noise characteristics of other types of silicon solar cells (i.e., different preparation techniques) should be evaluated to establish if the observed behavior in these experiments is typical for other types of cells.

INTRODUCTION

The development of a suitable encapsulation system for terrestrial photovoltaic arrays is a key requirement for the realization of the array cost and lifetime (20 years) goals of the Low-Cost Solar Array (LSA) Project[1] under which this study was carried out. The long-term integrity and stability of the encapsulation system will determine the operational lifetime of the array. The materials that provide this protection must be low in cost and must not significantly decrease the performance of the solar cells [2] There is, then, an urgent need for establishing reliable tests for characterizing the effects of weathering and time on the behavior of modules encapsulated with present and future encapsulation materials and systems.

A previous investigation by Battelle for the LSA Project was on the development of a "Methodology for Designing Accelerated Aging Tests for Predicting Life of Photovoltaic Arrays". The investigation (which is described in Report No. ERDA/JPL-954328-77/1) defined the need for and provides considerable background information for the study described in this report. That investigation developed an advanced methodology for designing accelerated aging tests for predicting the service life of terrestrial solar arrays. The existence of suitable instruments for measuring property changes associated with the degradation of array materials is an essential prerequisite to the successful application of any such methodology.

Instruments suitable for this application must provide sufficient sensitivity and precision to allow projections of ultimate system lifetime, and of performance over that lifetime, from short-time natural and/or simulated weathering tests. Sufficient confidence is required to allow selection among alternative designs and materials and to allow widespread use of such arrays Further, the diversity of candidate materials and designs, and the variety of potential environmental-stress combinations[3], degradation mechanisms, and failure modes will require identification of a number of combinations of measurement techniques that are suitable for characterizing various encapsulation system-environment combinations. To this end, currently used and potentially useful standard and developmental instruments and techniques have been examined to determine their applicability in lifetime-prediction testing.

Objective

It was the objective of this study to identify and evaluate instruments and techniques for measuring degradation-related changes in the properties of encapsulation materials and other module components that lead to array failure. Techniques are required for making accurate quantitative assessments of degradation rates for life-prediction studies.

Tasks performed in accomplishing these objectives included:

- Assessing the adequacy of existing instruments and techniques for meeting the diagnostic needs and measurement requirements of lifetime-prediction studies

- Identifying potentially useful techniques whose applicability required further evaluation through experimental testing

- Identifying diagnostic needs, if any, not adequately met by existing instruments and techniques or minor modifications thereof.

5

Approach

The study was conducted in two phases. Phase I consisted of a review and evaluation of measurement requirements and of potentially useful techniques and instruments on the basis of published literature, patents, reports, and discussions with specialists in relevant technical areas. The results and recommendations of that study are summarized in the Appendix of this report and greater detail is supplied in the interim report on this program.[4]

For the purposes of the Phase I review and analysis of instruments and techniques that might be useful in array-degradation studies, six general measurement-technique categories were established — chemical, electrical, optical, thermal, mechanical, and "other physical". Each of these categories was then assigned for study to a specialist in that area. This interdisciplinary team approach was used to ensure coverage of all potentially applicable techniques in the study. The specialists were responsible for collecting and reviewing published and unpublished information in their assigned areas, and subsequently for analysis of the applicability of the various techniques to array life-prediction testing. Key project staff members provided direction and close coordination of the team activities and statistical analyses and comparisons of techniques in the different categories. The information-gathering activities included computerized data-base searches, discussions with experts in specific instrument and technique areas, and a review of current periodicals and books

The information acquired through the computer-assisted data-base searches and the personal searches of current literature was augmented and amplified by discussions with outside specialists and equipment manufacturers for the key techniques (e.g., ultrasonics, IR spectroscopy, and dynamic mechanical) identified. The information developed from all of these sources provided the basis for the discussions, evaluations, and recommendations of the measurement techniques by the researchers for the interim report covering Phase I

In the overall approach to this study, it was necessary to assume that the focus was on measurement methods and instruments suitable for life-prediction testing and, specifically, for photovoltaic arrays. That is, the study could not cover the complete field of measurements and instruments, nor could it risk missing any diagnostic method that could be important to this specific use. To accomplish this, the interdisciplinary project team pursued as a group the following steps in Phase I:

(a) Identification of all observed and projected *failure types/modes* for photovoltaic arrays and materials

(b) Organization and breakdown of major failure types, identifying all possible subtypes and the *degradation factors* and *causes* involved in the failures

(c) Identification of the microscopic *degradation mechanisms* possibly leading to each of the types of degradation and failure

(d) Definition of the microscopic and macroscopic *property changes* that might be associated with these degradation mechanisms

(e) Identification and analysis leading to specific recommendation, of the *measurement techniques/instruments* which might be used for early detection of these degradation-related property changes

6

One important result of the first phase of the work was the recommendation of a number of techniques which were judged to be potentially useful in degradation studies, but which required further evaluation to fully assess their suitability, applicability, and potential advantage. These recommendations provided the basis for Phase II activities.

Phase II involved a preliminary experimental evaluation of the applicability of three of the techniques recommended in Phase I. Selections were made on the basis of potential advantage either in sensitivity relative to currently used techniques or adaptability to "in-the-field" measurements The techniques selected were optical reflectance and light scattering measurements for characterizing interface changes and defects, chemiluminescence measurements for early detection and characterizations of ultraviolet radiation-induced changes in polymers, and electrical noise measurements for characterizing series resistance changes in cells and modules. A discussion of the preliminary experimental evaluation of these techniques forms the main body of this report.

PHASE II EXPERIMENTAL EVALUATIONS

The three techniques (specular and nonspecular optical reflectometry, chemiluminescence, and electrical noise) evaluated in this phase of the study were selected from a number of techniques recommended for further investigation as a result of the Phase I findings. While these techniques were selected because they were felt to offer specific advantages in the study of degradation in photovoltaic modules, their selection is not intended to indicate superior merit or greater importance relative to the other techniques recommended in Phase I. Many of the other recommended techniques are judged to be of at least equal merit; however, the limited scope of the Phase II effort prevented their evaluation as part of this study. It is hoped that other researchers within the photovoltaic community will find the interest and support to pursue some of the other recommended techniques.

Two desirable characteristics of measurement techniques for use in degradation and life-prediction studies are high sensitivity to properties measured and adaptability to on-site measurements. The techniques studied in Phase II embody one or both of these characteristics, which is one of the reasons they were selected. The electrical noise measurements, and some of the optical techniques investigated, offer clear potential for on-site use, while chemiluminescence is potentially one of the most sensitive techniques for studying oxidative and UV-induced changes in polymeric structures. In addition, studies of the electrical noise characteristics of other types of semiconductor devices indicated that this type of noise may offer a more sensitive means of characterizing series-resistance changes associated with contact corrosion or debonding than more conventional approaches. Other considerations which influenced the selections for specific applications are further elaborated in the following discussions

Optical Reflectance Experiments

Background

Several types of environmentally induced degradation can affect the intensity and angular distribution of light reflected from a damaged surface or interface. Potential causative factors include delamination, consequences of abrasive particle impact, and surface or bulk effects resulting in refractive index changes. Measurement of the specular and nonspecular reflectance could provide a basis for early detection and quantitative characterization of these degradative changes. It has been reported[5], for example, that certain types of first-surface damage can be detected, although not fully characterized, on glass and polymer cover sheet materials by simply measuring the reduction in specular reflectance. Direct measurement of the scattered light provides more information, but in some cases, has required metallization of the surface for accurate results.[6]

Delamination is one of the major concerns in present-day photovoltaic modules. Several optical techniques are applicable to the detection and characterization of this type of failure.[7] The relative simplicity with which reflectance measurements can be implemented and their nondestructive nature gives them a high potential for use in in-situ evaluation of delamination. The ability to distinguish between various degradative effects is probably one of the most difficult tasks. Reflectometry is one of the tools that can be brought to bear on this problem.

On the basis of the above considerations, an initial investigation of specular and nonspecular reflectometry for evaluation of degradative phenomena at interfaces was recommended. In view of the limited scope of the effort and the importance of delamination as one of the major defects observed in the field, it was recommended that these experiments focus on delamination

Delaminations have been observed in many types of encapsulated solar-cell arrays, but aside from their generally small effects in reducing the amount of light reaching the junction, their influence on long-term cell and array performance is not clear. Commercial arrays undergoing field tests for up to 2 years contain numerous delaminated areas, but these do not appear to have affected array output over this period. Delaminated areas are nontheless legitimate objects of concern, since they could clearly lead to acceleration of long-term degradation, for instance, by providing sites for prolonged attack of AR coatings, metallization, and interconnects by water vapor (or liquid) and pollutants

But because the mechanisms by which delamination may lead to degradation are largely unknown, it is not possible to specify those characteristics of delaminations that should be recorded as a function of exposure time (under normal or accelerated stresses) in order to predict the degradation rate of power output. Among the characteristics of delaminations that might conceivably be quantified by optical methods are:

(1) Number per unit area

(2) Average size

(3) Distribution function of given size per unit area [when (1) and (2) are not sufficient to give a description of the observed distribution]

(4) Shape (circular, elliptical, irregular, etc)

(5) Location (over metallization, at cell edges, near interconnects, near binding posts, etc.)

(6) Degree of separation (maximum)

(7) Transverse cross section

(8) Presence of material (debris, water, droplets) within delaminations.

Optical inspection methods that might be applied for detection and characterization of delaminations are:

(1) Visual inspection

(2) Microscopic examination

(3) Reflection methods

(4) Holographic methods

(5) Light scattering.

Simple visual inspection is the least time-consuming method and is carried out routinely during field testing. However, such inspection is suitable for detecting only rather obvious delaminations. On the other end of the scale, sufficiently painstaking microscopic work should detect — and at least in part characterize — all delaminations greater than 1 μm or so in diameter. One objective of the present work was to determine if any of the other methods listed above offered useful alternatives or adjuncts to these two. Only non-destructive tests were considered. Suitability for adaptation to field work was also considered, but development of experimental designs for this consideration was not emphasized at this early stage.

9

Samples Used and Experiments Conducted

Cells encapsulated in several ways were used as test samples. Generally, test samples with some obvious delaminations were selected. No attempt was made to further degrade the cells Encapsulant systems included.

(1) Acrylite cover plate - Scotchweld adhesive

(2) PPG float glass cover plate - Sylgard 184 encapsulant

(3) 7740 Pyrex glass cover plate - Q36520 gel encapsulant

(4) No cover plate - GE RTV 615 silicone encapsulant

Test-samples of the first type delaminated severely between the cover plate and the Scotchweld upon temperature cycling or exposure to high humidity In the other test samples, delaminations tended to occur between the encapsulant and the cell antireflection coating, or between the encapsulant and the back insulating layer in regions between cells. Test samples of the first three types listed above were encapsulated at Battelle, the silicone-encapsulated cells were from Solarex modules removed from the Mead, NB, array.

Specific experiments included

(1) Overall reflection and imaging of an expanded coherent beam

(2) Point-by-point reflectometry

(3) Double-exposure holographic interferometry

(4) Imaging of scattered light by spatial filtering of a reflected coherent beam

(5) Light scattering from a tangential beam propagating parallel to the cell surface.

Not all experiments were performed on all types of test samples. Each of the experiments is discussed in turn, the results are summarized, and the conclusions presented

Interface Reflectivity

The most straightforward method for improving the visibility of delaminations is examination of the cell in monochromatic light. Delaminated regions show up as areas with irregular interference fringes resulting from multiple reflections. In this study, experiments along this line consisted of expanding the beam (0 488-μm wavelength) from an argon-ion laser to the diameter of the cell or a little more, reflecting the beam from the cell, and examining and photographing the reflected image. An example of such an image, taken on a Scotchweld-Acrylite module that had severely delaminated over the cell-proper, is shown in Figure 1 A small elliptical region of separation, less than 1 mm in its greatest dimension, is indicated by the arrow. Small delaminations like this are easily missed in visual inspection, although they can be seen readily enough when one knows they are there For the Scotchweld-Acrylite test samples, the contrast between delaminated and bonded regions is high in the blue argon-laser light because this light is strongly absorbed by the adhesive layer Such a good contrast ratio cannot, of course, be expected when test samples of different composition are examined by this technique. Scotchweld-Acrylite encapsulated test samples also often have small delaminations between the adhesive layer and the cell or the backing plate These delaminations will not generally be visible using the technique just described, but they might be seen by repeating the experiment using red light, or by one of the other methods to be described

10

FIGURE 1. COHERENT–LIGHT IMAGE OF SEVERELY DELAMINATED
ACRYLITE-SCOTCHWELD ENCAPSULATED CELL

Dark areas are regions of good adhesion between cover plate and
adhesive. A small delamination lies directly beneath the arrow.

More detailed information about the reflectivity at a given interface can be obtained through point-by-point measurements. A simple system for such measurements is illustrated in Figure 2. The source, a He-Ne laser beam of 0.6328 μm wavelength, is focused to a spot of less than 50 μm diameter at the test sample surface. The reflection from the front surface is blocked off and only the beam reflected from the AR coating-encapsulant interface is detected. (Test samples with large index differences or delaminations between cover plate and encapsulant have not been used in these experiments.) The position of the cell with respect to the light beam is converted to a voltage by means of a gear arrangement and a potentiometer; this voltage is sent to the x-axis input of an x-y recorder, while the output of the photodiode is sent to the y-axis.

The recorder outputs for single traverses of two different test samples are shown in Figures 3 and 4. The traverse locations were selected to cross interesting features such as metallization stripes and obvious delaminations. The output signal has not been accurately related to the true interface reflectivity; however, the range indicated by the scale on the left-hand edges of the figures corresponds to about 1 or 2 percent reflectivity. The effect of metallization on the reflectivity can be readily observed in both traces. The traverse of Figure 3 crossed several secondary metallization fingers, while that of Figure 4 crossed only the main collector. Delaminations effect a large increase in the reflectivity by adding an encapsulant-to-air interface above the AR coating. In addition to these features, a number of other regions of increased reflectivity are apparent in both traverses. Some of the more prominent of these are indicated on Figures 3 and 4. These regions do not correspond to any features apparent on microscopic examination; it is possible that they represent incipient delamination areas.

Originally, it was hoped that some quantitative information about the shape of the delaminated adhesive surface could be obtained from measurements of this type. This did not prove possible with the experimental arrangement described above. A more sophisticated system, with a wide-range linear detector, ratio recording, and careful elimination of stray light, should provide useful results in this regard. It is also possible that the reflectivity jumps to its maximum value very close to the delamination edge and maintains very nearly this value regardless of changes in the delamination thickness. Neither the present results nor microscopic examination of the delaminations gives any reason to expect anything different.

While interface reflectivity is clearly capable of providing information that can be obtained in no other way, an adequate statistical survey of just a single cell requires considerable time, even if the work is automated as much as possible. The relationship of any of the features observed to delamination rate also needs to be established for each type of module of interest.

Double Exposure Holography

The experimental arrangement used for double-exposure holography experiments is shown in Figure 5. The source, an Ar-ion laser, can be made to emit intensely at wavelengths of either 0.4880 μm or 0.5145 μm. The former wavelength is used to write and read out the holograms, while the latter is used only as a convenient source for heating the sample. A crystal of LiNbO$_3$ is used as a phase-sensitive recording medium. The experimental procedure is as follows:

(1) With shutters S1 and S2 open and S3 closed, a holographic image of the cell is made and recorded in the LiNbO$_3$

(2) With S1 closed and S3 open, the module is heated for several minutes using the 0.5145 μm beam
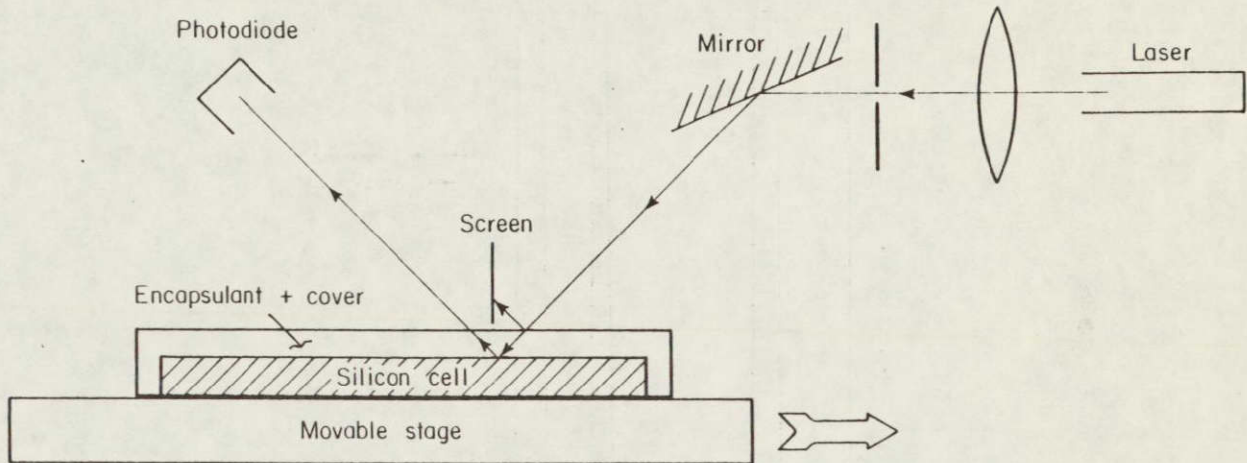
FIGURE 2. EXPERIMENTAL ARRANGEMENT FOR POINT–BY–POINT MEASUREMENTS OF REFLECTIVITY AT INTERFACE BETWEEN ADHESIVE OR ENCAPSULANT LAYER AND ANTIREFLECTION COATING OF SILICON SOLAR CELL

Not shown are the system for electrically sensing relative stage position along direction indicated by arrow and the X–Y recorder on which photodiode output is plotted as a function of stage position.
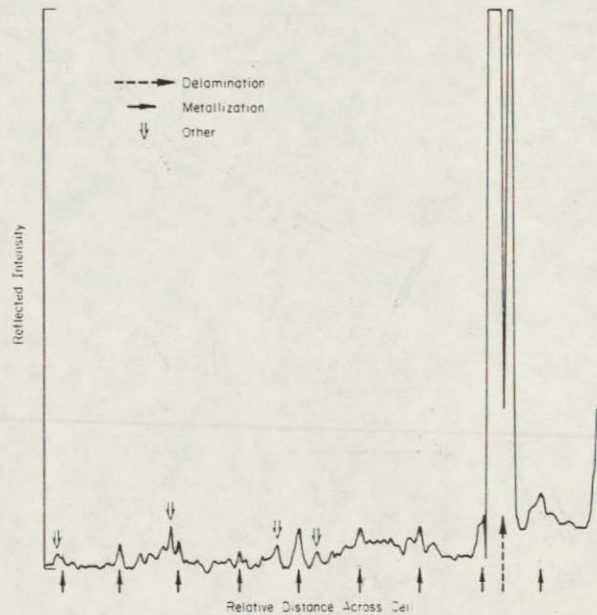
FIGURE 3. REFLECTION AT ENCAPSULANT–AR–COATING INTERFACE ALONG TRACK 50 μm WIDE CROSS FLOAT–GLASS–SYLGARD ENCAPSULATED SOLAR CELL

Scale at left corresponds to roughly 1 or 2 percent reflectivity change. The recorder is saturated at top of graph. Effects of metallization and delamination on reflectivity are indicated by arrows as well as some other reflectivity peaks of unknown origin.

13
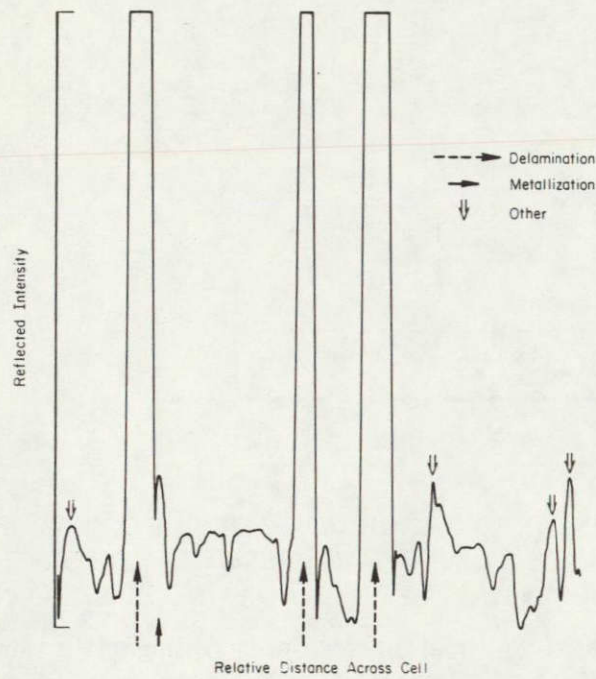
FIGURE 4. INTERFACE REFLECTIVITY AS IN FIGURE 3, BUT FOR PYREX–Q36520–GEL ENCAPSULATED CELL
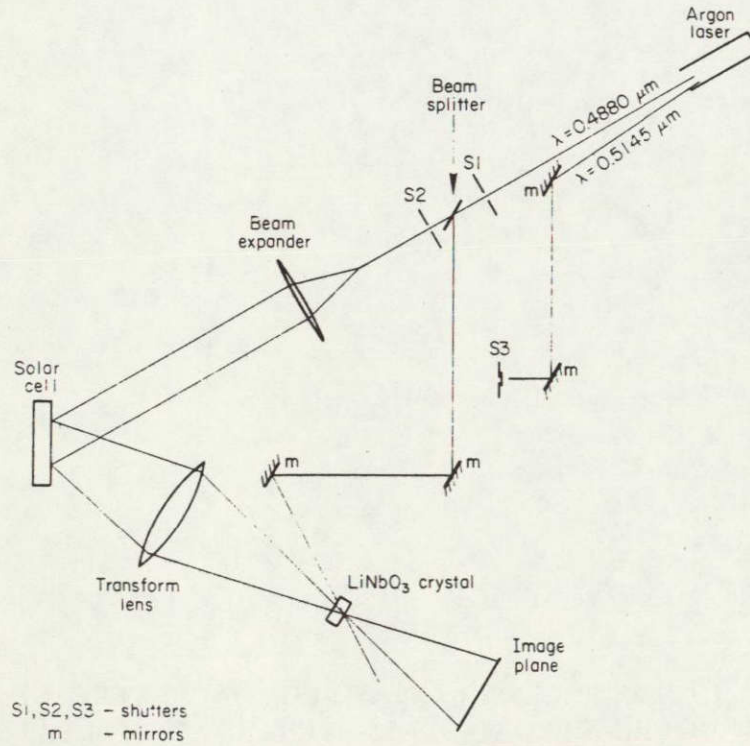
FIGURE 5. EXPERIMENTAL ARRANGEMENT FOR DOUBLE–EXPOSURE HOLOGRAPHY OF ENCAPSULATED SOLAR CELLS

(3) With the shutters as in the first step, a second hologram, of the warm cell, is made and recorded on top of the one already present in the LiNbO$_3$

(4) With S2 and S3 closed, the double-exposure hologram is read out and photographed.

Heating the sample is expected to lead to non-uniform expansion in the neighborhood of flaws such as delaminations. The consequent local phase changes in the reflected beam will make these features visible in the holographic image. An image of a float glass/Sylgard encapsulated cell is shown in Figure 6. A large, irregular, delaminated area can be seen at the lower right edge of the cell. Some other delaminations that were expected to be seen were not evident. The center of the photograph is overexposed owing to the spatial inhomogeneity of the laser beams. The fringe pattern near the center at the bottom is believed to be an imperfectly erased earlier hologram in the LiNbO$_3$. Of the other features evident in the hologram, the most prominent is a row of spots running vertically near the left edge of the cell. Microscopic examination showed that these are probably subsurface cracks near the front face of the float glass. Figure 7 is photomicrograph of one of these features. It appears that at sometime, the float glass was gripped or impacted with a row of pointed or finely cylindrical objects that produced the cracks, whose location below the surface might be due to the presence of a surface layer harder than the bulk.

With certain improvements, such as better beam apodization, and possibly a more effective heating method, this technique could be effective in revealing delaminations and other defects over rather large areas. However, it has certain drawbacks. For one thing, a certain amount of experimentation is required to determine satisfactory levels of recording beam intensity and degree of heating or other stress, since the characteristics of the defects being sought will not generally be known a priori. Also, when defects are located, additional investigation is required to determine the level above the cell surface at which they occur.

Light–Scattering Methods

Two light-scattering methods for investigating delaminations were studied. The first of these involves reflection of an expanded coherent beam from the test sample, as in the simple reflection experiment described above. However, a spatial filter is inserted to block the specularly reflected beam so only the light scattered by imperfections is imaged. The experimental arrangement is shown in Figure 8. This technique successfully revealed numerous small scattering sites in the encapsulating layers and at their surfaces. As an example, Figure 9 shows a scattered-light image of the same cell that was used in the double-exposure holography experiments. Numerous scattering centers, including the row of subsurface cracks described earlier, became evident in the well-illuminated portion of the cell. Few of these centers were associated with any observable defects at the adhesive/AR coating interface; it seems likely that most of them were located at or near the cover-plate surfaces.

This method was not completely successful in revealing larger delaminated regions readily apparent on visual inspection. As with the holographic method, additional work is required to locate the plane of the defects observed. It also seems rather difficult to tell which of the many scattering sites are associated with the most prominent defects.

The other scattering method investigated consisted of propagating a laser beam through the encapsulant parallel to, and very close to, the AR coating, and observing light scattered by defects through the front face. The experimental setup is shown in Figure 10. The beam may be injected directly through an opening in module or test sample wall, or it may be introduced through an

15
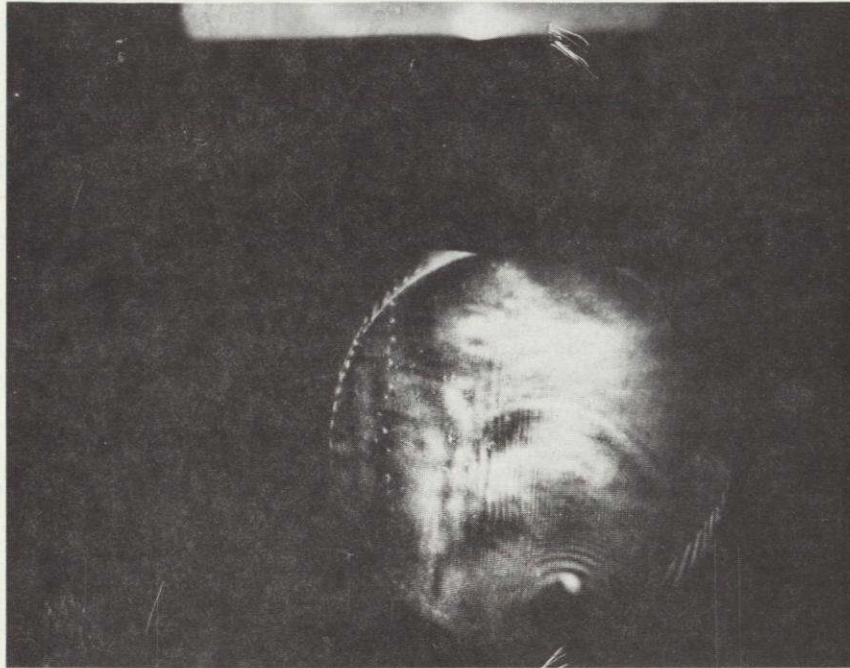
FIGURE 6. DOUBLE–EXPOSURE HOLOGRAM OF A FLOAT–GLASS–SYLGARD ENCAPSULATED CELL
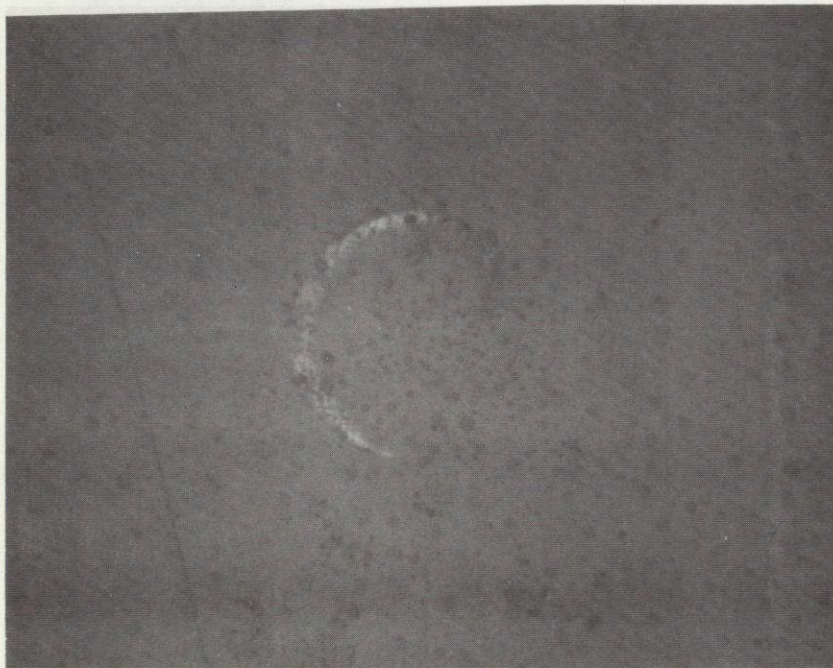
FIGURE 7. BRIGHT–FIELD PHOTOMICROGRAPH OF SUBSURFACE DEFECT, POSSIBLY CRACKED REGION, IN FLOAT GLASS

Magnification about 45X

16
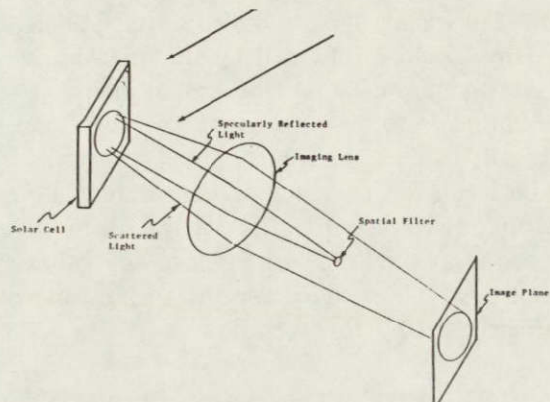
FIGURE 8. EXPERIMENTAL ARRANGEMENT FOR OBSERVATION OF SCATTERED LIGHT BY SPATIAL FILTERING
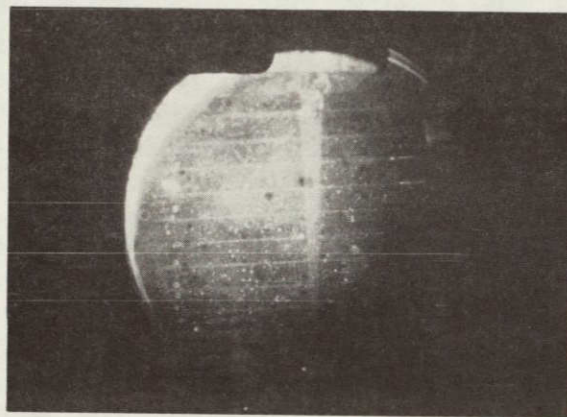
FIGURE 9. SCATTERED-LIGHT IMAGE OF SAME ENCAPSULATED SOLAR CELL SHOWN IN FIGURE 6
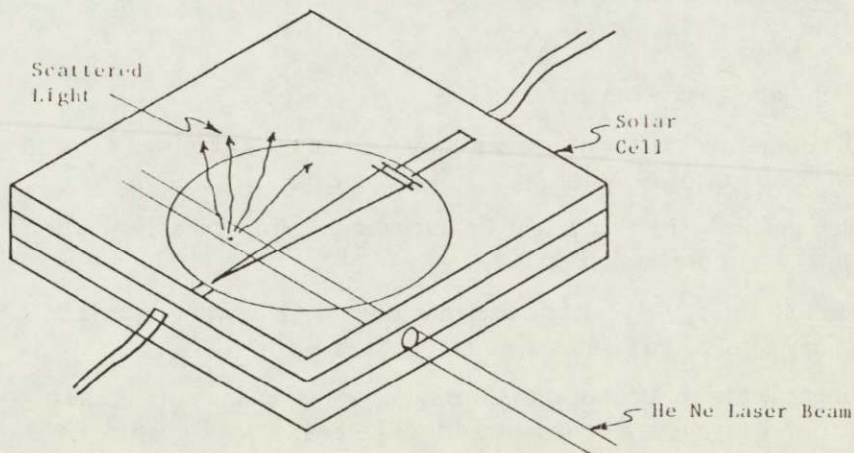
FIGURE 10. EXPERIMENTAL ARRANGEMENT FOR STUDYING LIGHT SCATTERING AT INTERFACE USING TANGENTIAL BEAM

17

optical fiber. In either case, by sweeping the beam back and forth within the adhesive layer, the adhesive/AR coating interface of a test sample may be examined for delaminations and other defects in a very short time. This procedure can locate defects that are quite difficult to find by visual inspection. For instance, a defect readily found in one cell by this method was subsequently examined microscopically (Figure 11) and found to be only about 50 μm in diameter. It should be noted in passing that a defect like this, which appears to be a pinhole into the silicon along with some associated surface damage, is very difficult to describe quantitatively in terms like those given above. More importantly, the relationship between the presence of such defects and future delaminations or other degradative mechanisms is unknown. Examination of the entire adhesive/AR coating interface of this cell by dark-field microscopy at 65X did not disclose any other sizable scattering centers, except for a few gross delaminations. Thus, there appears to be some reason to believe that the more significant scatterers can be singled out by this technique.

This method was also tried on three silicone-encapsulated cells in a Solarex module removed from the Mead, Nebraska installation. The silicone had been cut away over one cell, enabling the beam to be injected at the cell-encapsulant interface of adjacent cells using an optical fiber. After traversing only one 5-cm-diameter cell, the beam was too greatly attenuated by scattering from the metallization to be useful. More than a dozen strongly scattering features were noted on the three cells or in the spaces between them. These scattering sites were marked and were subsequently examined with an 8X hand lens. The majority of scatterers appear to be sizable spots (up to 0.5 mm in maximum dimension) of excess metallization between the collectors. These cells also contain numerous smaller bits of excess metallization from which weak light scattering was observable. Of the other scattering centers, one was an extended cloudy area in the silicone, one was a bubble in the silicone a little above the interface, and two appeared to be small delaminations, about 0.2 to 0.3 mm in diameter. Some scattering sites did not correspond to anything that could be observed with the hand lens. One apparent larger (0.5 mm x 1 mm) delaminated area did not scatter light effectively.

In addition to the advantages mentioned above for this technique, it also has the great advantage of examining a single interface. If it is to be implemented as a test method, though, means for ingress of the laser beam to each cell will have to be provided, without compromising the integrity of the encapsulation.

Conclusions on Specular and Nonspecular Optical Reflectance Techniques

Conclusions from the above experiments are:

(1) Regions of delamination exist that are not apparent on cursory visual inspection. This is true of a variety of types of encapsulant systems.

(2) Other interface defects exist that might be nucleating points for delaminations under additional environmental stress.

(3) Regions of altered reflectivity exist at the encapsulant/AR coating interface. Such regions may also be incipient delamination sites.

(4) All the methods tried were successful in showing up some delaminations and other defects, but none alone revealed all features judged to be of possible interest.
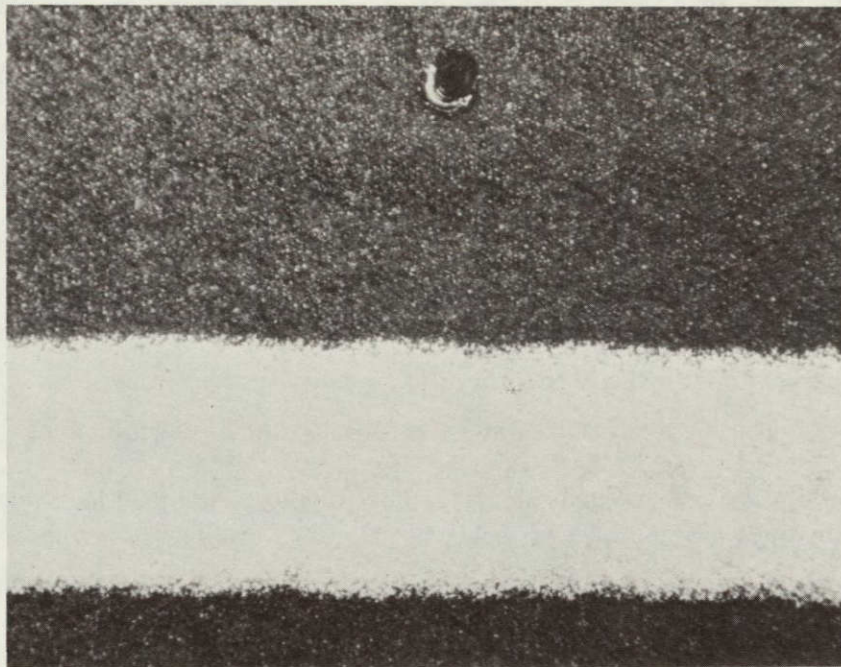
FIGURE 11. UNUSUAL DEFECT AT SYLGARD–AR–COATING INTERFACE DETECTED BY TANGENTIAL-BEAM LIGHT SCATTERING

Secondary metallization finger at bottom of picture. Dark–field photomicrograph at about 90X magnification.

(5) The types of optically responsive defects encountered are sufficiently numerous and varied that no method short of detailed mapping and measurement seems likely to be useful for following the progress of delamination during accelerated tests.

(6) The most generally useful adjunct to simple visual inspection appears to be tangential-light-beam scattering, as described above. Provision has to be made, though, for getting the tangential beam into the cell of interest; if the cell is part of a module, this could pose difficulties.

The requirements, other than the basic optical equipment, for performing any of the tests described are simple: darkness, a relatively vibration-free environment, and a small amount of electrical power. Satisfying these requirements in a true field-test configuration is probably out of the question, but on-site testing of modules removed from an array should not be difficult.

In view of the present rudimentary state of knowledge concerning what ought to be looked for in delamination testing, it is difficult to make any specific recommendations. Among considerations for a given type of encapsulant system in which delaminations are suspected of leading to degradation are:

(1) Whether degradation is related to number, size, or location of delaminations

(2) Whether delaminations are likely to form or to grow under accelerated stress

(3) Which types of areas are likely nucleation sites for initiation of delaminations.

Given this information, optical test methods along the lines of those described here might be usefully applied to delamination studies.

Chemiluminescence Experiments

Background

Many properties of polymeric encapsulants change as a result of environmental aging. These changes manifest themselves at some point in the degradation process as macroscopic property changes such as embrittlement, discoloration, and increased dielectric loss. However, long before property deterioration is apparent, the degradative processes are active and chain-scission, crosslinking, and other types of chemical reactions are occurring at the molecular level.

The identification and development of techniques to detect these molecular changes very early in the degradative process is desirable. This requirement for early detection of very small changes is illustrated in Table 1. One promising method for such detection is chemiluminescence, the measurement of electromagnetic radiation in the visible spectrum that is generated when an organic material reacts with its environment. This technique has a distinct advantage over most other analytical tools utilized in structural characterization; it can detect chemical reactions that are occurring at rates as low as 10^{-14} mole per year.

The objective of the experiments described in this section was to correlate chemiluminescence measurements with UV-induced degradation mechanisms in polymers in order to establish the usefulness of the technique in characterizing degradation rates. Since such measurements are known to be very sensitive to small physical and/or chemical changes in materials, it was considered important

20
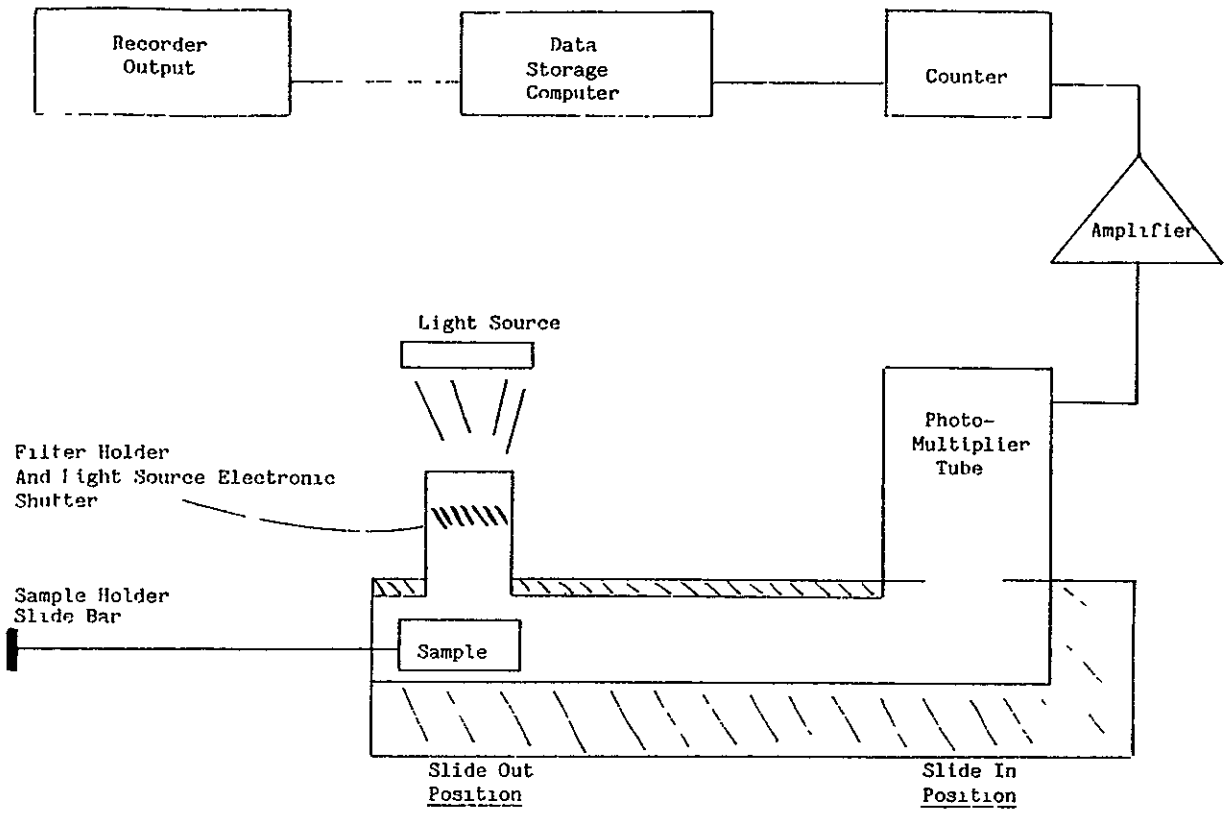
FIGURE 12. CHEMILUMINESCENCE APPARATUS

(3) The irradiated sample was placed under the photomultiplier tube (slide in) for analysis.

(4) Photomultiplier counts were recorded following a 15-second delay after light exposure of the sample

(5) Data output was recorded in the form of a plot. counts per second (intensity) versus seconds (time)

Experimental Results and Discussion

Figure 13 shows traces of chemiluminescence output versus time for the control sequences. These traces were run in order to check the apparatus for stray, long-lived, background luminescent transients (electronic noise, impurities, light reflection, etc). Measurement conditions are shown with the figure. In all cases, no long-lived transient signal could be detected. Identical traces were obtained in both nitrogen and air atmospheres.

Direct irradiation (unfiltered Hg lamp) of a nitrogen-blanketed, PMMA sample (10-second exposure followed by a 15-second delay before recording a photomultiplier tube output signal) resulted in a long-lived decay curve (Figure 14 - Run 1). The control run (irradiation of the sample holder without shutter closed followed by photomultiplier tube detection analysis) showed no sign of signal decay and resulted in a flat baseline curve Continued irradiation of the same sample for an additional 10 seconds (cumulative irradiation exposure of 20 seconds) followed by photomultiplier tube analysis resulted in a decay curve similar to the previous experiment (Figure 14 - Run 2). Further irradiation of the same sample (cumulative irradiation time of 40 seconds) under the same experimental conditions gave a somewhat higher signal intensity, but the decay curve was very similar to those of Runs 1 and 2 (Figure 14 - Run 3). Figure 15 shows a scale expansion of the decay curve for Runs 1, 2, and 3 allowing ease of data point selection for graphical analysis.

In Figure 16, the traces for PMMA decay curves are shown after 20 seconds' exposure time – Run 4 (cumulative irradiation of 60 seconds), 30 seconds' exposure time - Run 5 (cumulative irradiation of 90 seconds), and 10 seconds' irradiation - Run 6 (cumulative exposure of 100 seconds). Scale expansion for Runs 4, 5, and 6 are shown in Figure 17. Experimental Runs 1 through 6 and their controls were carried out in a nitrogen atmosphere.

Plots resulting from studies of effects of irradiation wavelength dependence and exposure time on PMMA and its decay curve in an air atmosphere are shown in Figures 18 through 22. A series of light filters was used to isolate the stimulating wavelength associated with inducement of the observed decay curve emission (Figure 18). Pure PMMA has UV absorption only at 254 nm. A Corning filter No. 3387 (excludes all wavelengths below 440 nm), placed between the mercury light source and the PMMA sample, did not produce a long-lived transient but resulted only in a flat control baseline after 10 seconds' exposure time (Figure 18 - Run 2). Nor was a long–lived decay curve observed when a pyrex filter (excludes all wavelengths below 280 nm) was placed between the light source and the PMMA sample (Figure 18 - Run 3) Only quartz (open or unshielded Hg light source in a quartz water jacket), which allowed passage of the 254 nm excitation wavelength, produced an observable decay curve (Figure 18 - Run 1)

23
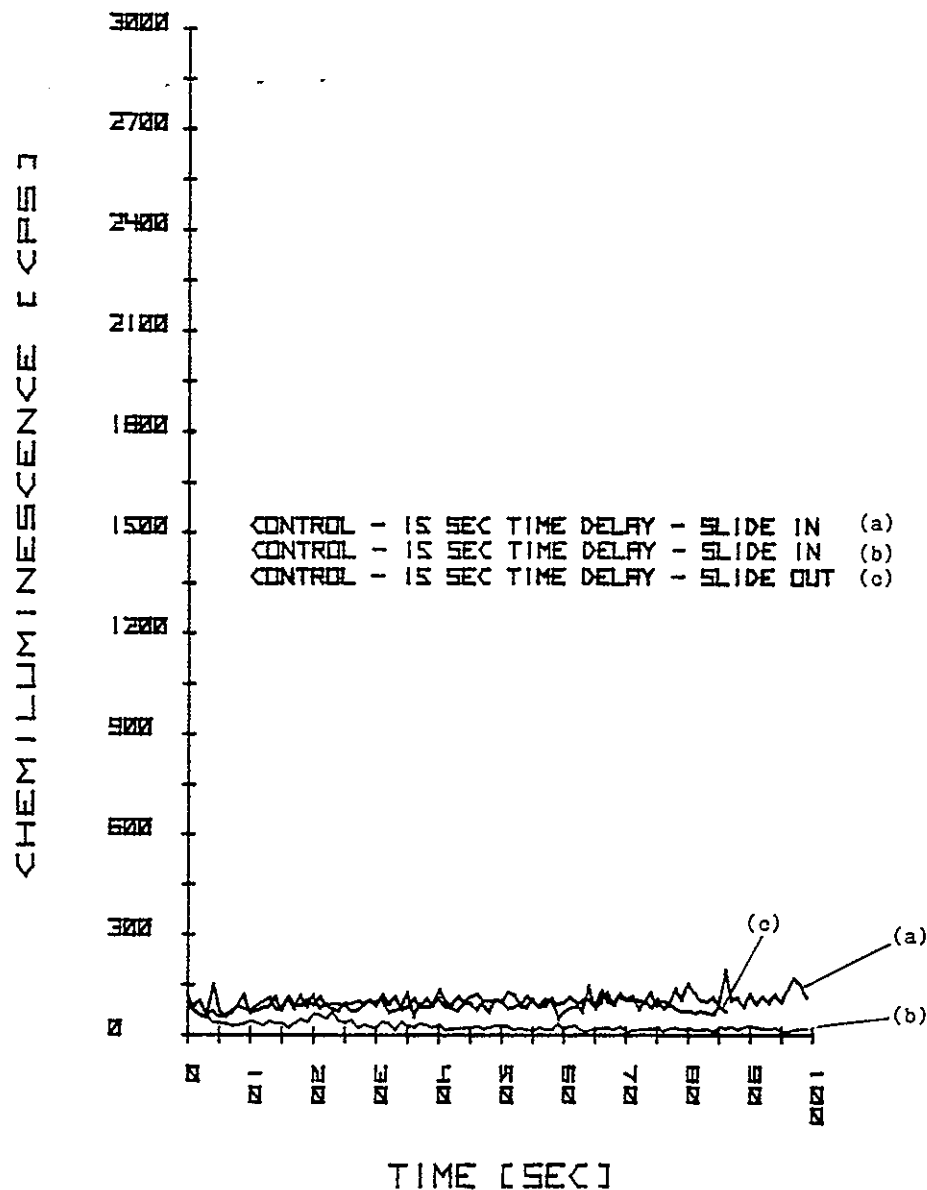
FIGURE 13. PLOT OF CHEMILUMINESCENCE INTENSITY (COUNTS PER SECOND) VERSUS TIME (SECONDS) FOR CONTROL RUNS

(a) No irradiation with the slide sample holder empty or containing the PMMA sample placed directly under the photomultiplier tube followed by a 15-second delay before recording output signal, (b) Same as (a) but with irradiation and closure of electronic shuttle, (c) Irradiation with the electronic shutter closed and the sample slide holder containing PMMA remaining out away from the photomultiplier tube.

24
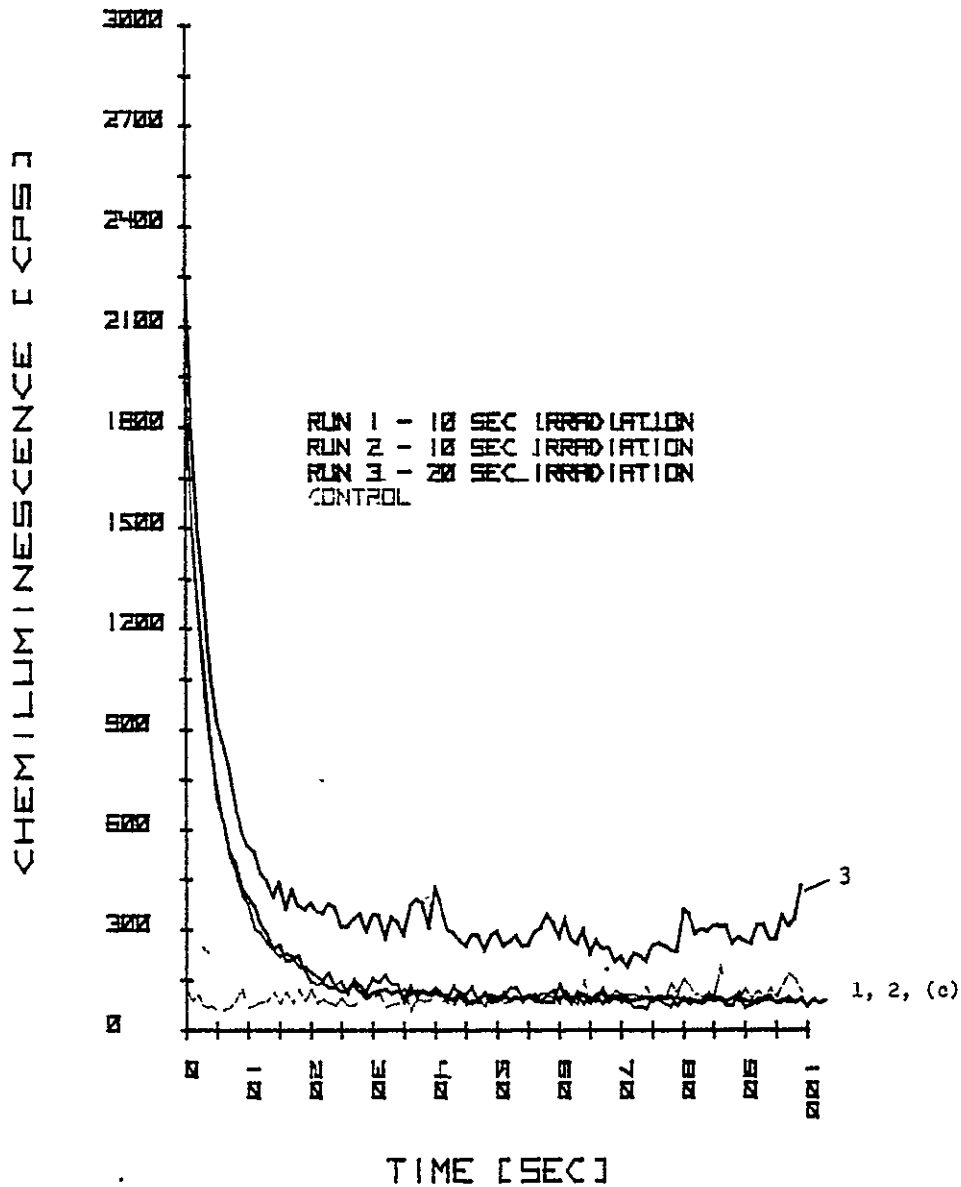
FIGURE 14. PLOT OF COUNTS PER SECOND (CPS) INTENSITY
READINGS FOR IRRADIATION OF A SINGLE PMMA
SAMPLE

The individual runs (1, 2, and 3) had 10, 10, and 20 seconds
exposure time leading to a cumulative exposure time of 40
seconds for the PMMA sample.

25
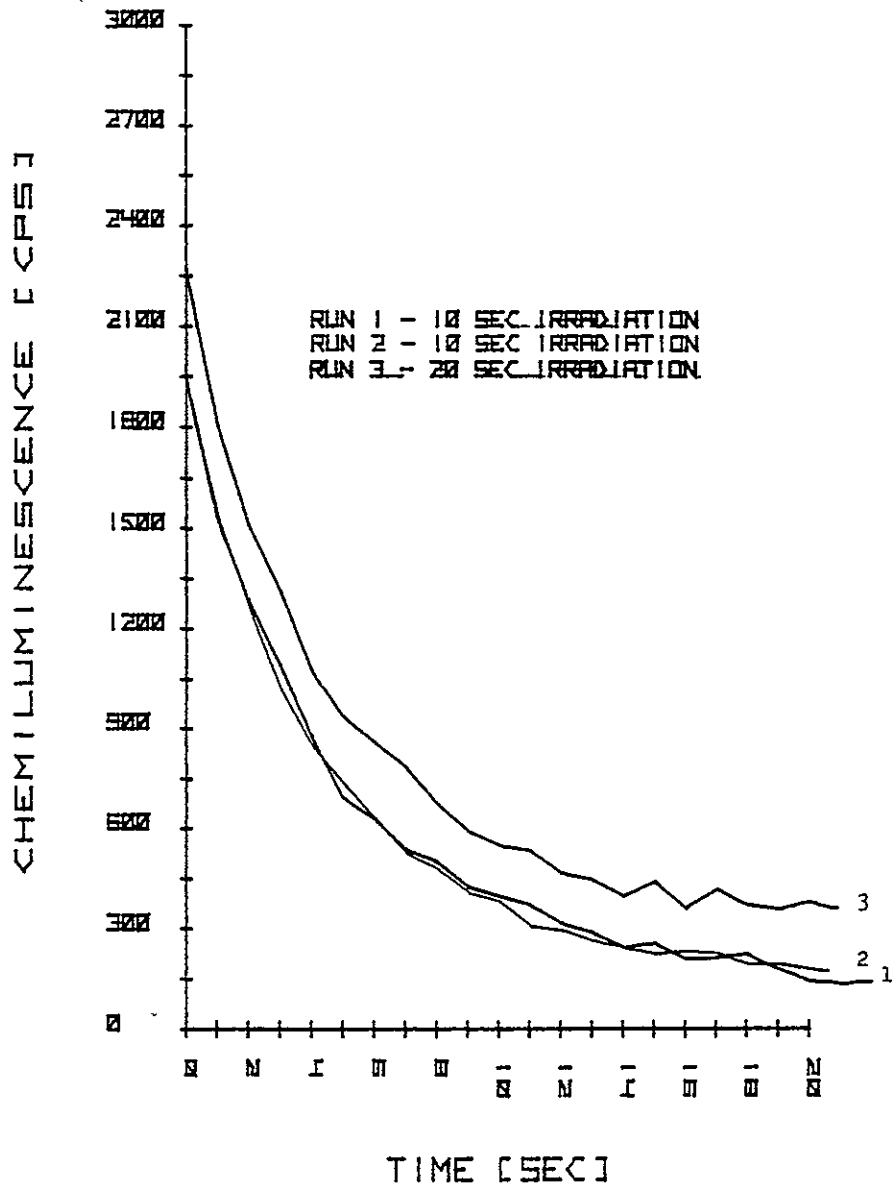
FIGURE 15. SCALE EXPANSION OF FIGURE 14

NASA
FORMAL
REPORT
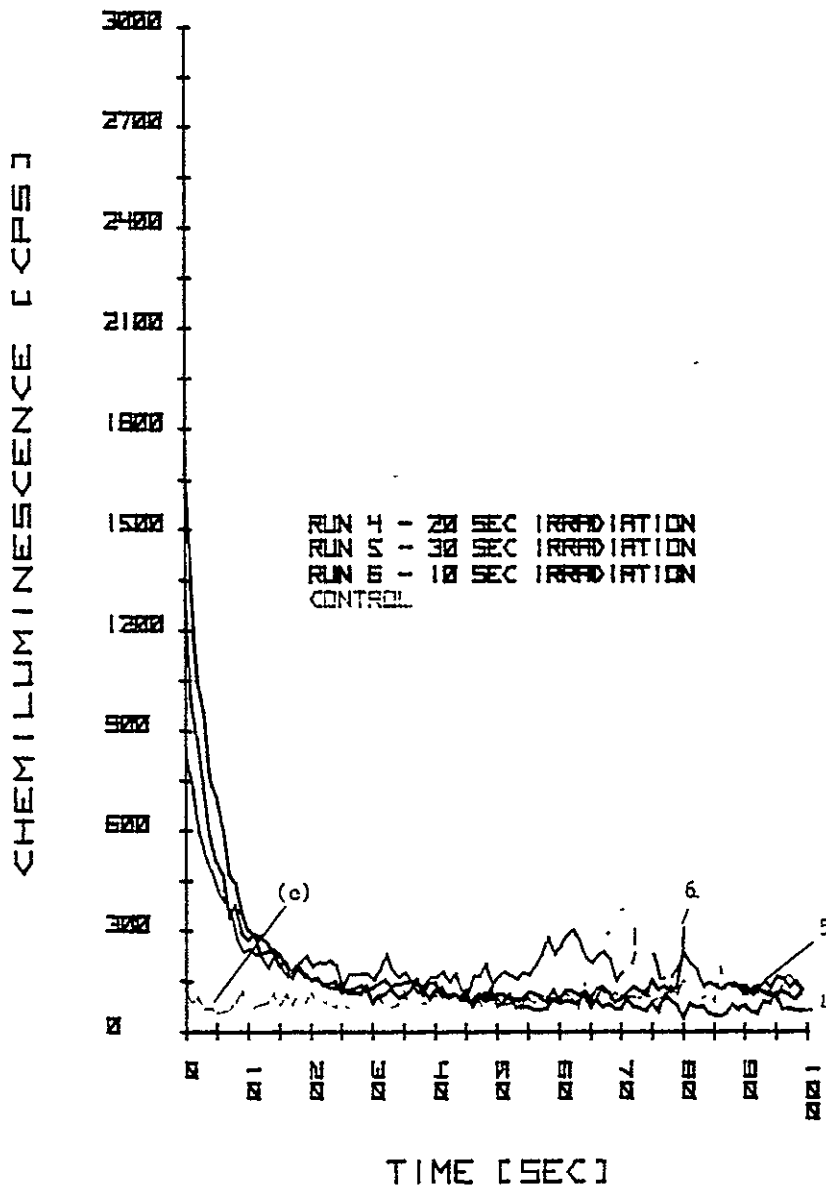
FIGURE 16. PLOT OF CPS VERSUS TIME (SECONDS) FOR
CONTINUED IRRADIATION OF THE PMMA
SAMPLE UNDER NITROGEN ATMOSPHERE

The individual runs (4, 5, and 6) had 20, 30, and
10 seconds exposure time leading to a cumulative
total of 100 seconds.

27
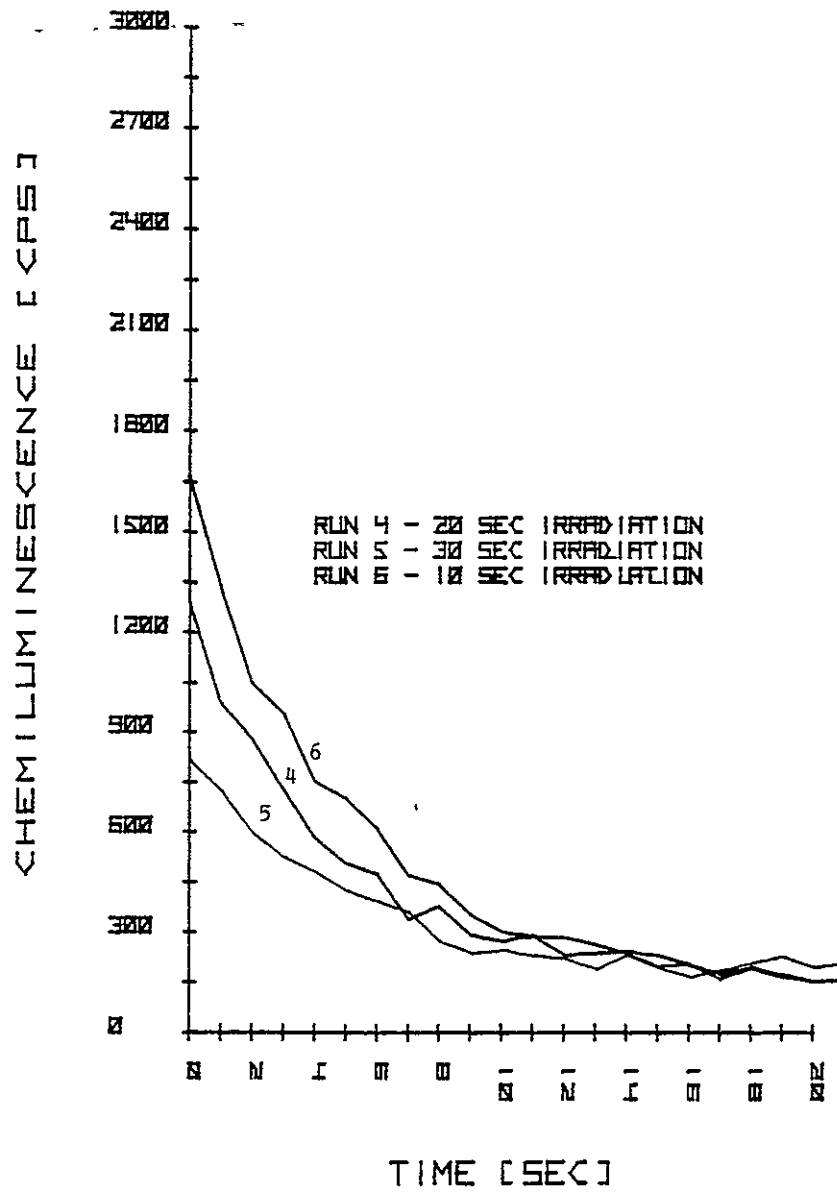
FIGURE 17. SCALE EXPANSION OF FIGURE 16
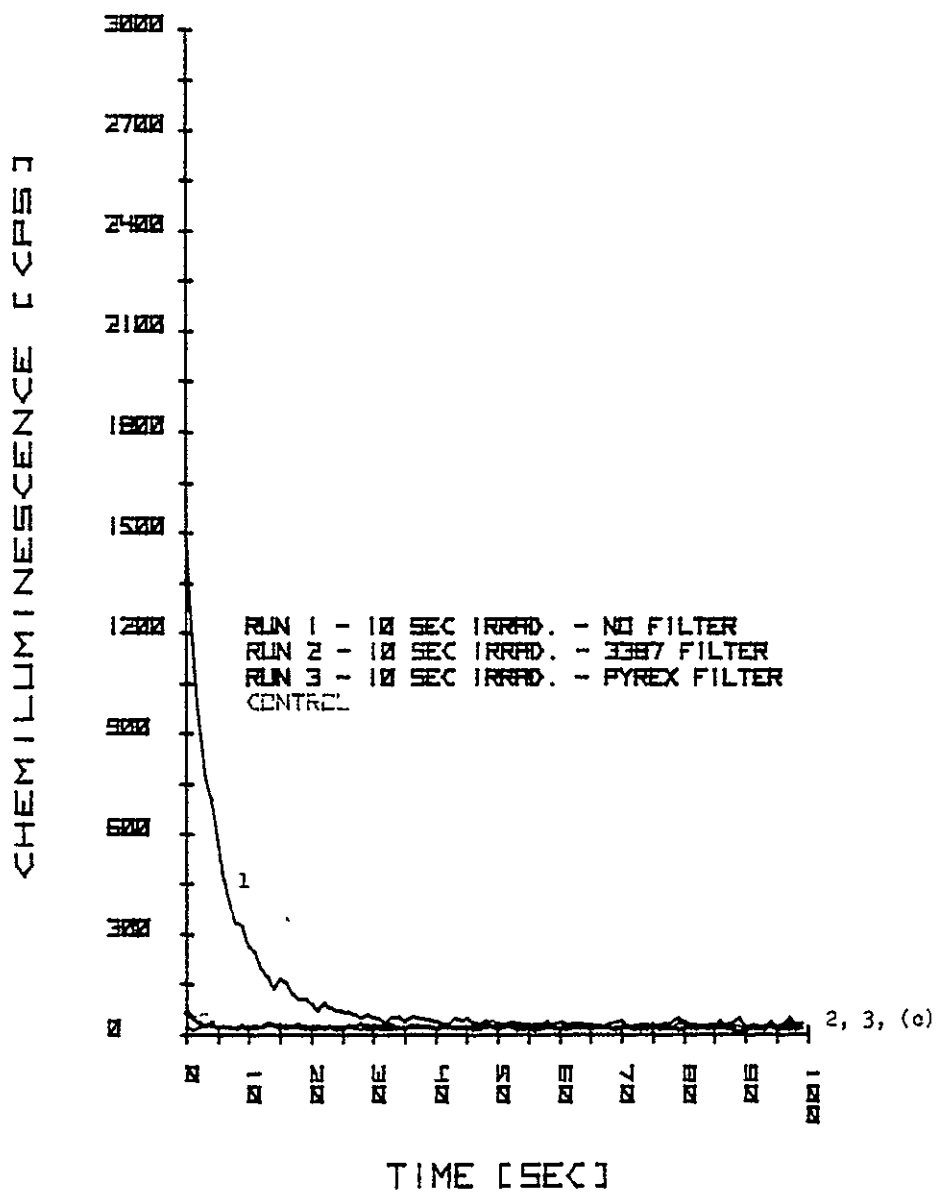
FIGURE 18. INTENSITY PLOT OF CPS VERSUS TIME FOR
PMMA IRRADIATION IN THE PRESENCE OF AIR

Run 1 consisted of sample exposure to 254 nm
UV-radiation for 10 seconds. Runs 2 and 3 utilized
a 3387 corning filter and a pyrex glass filter, respectively.

29

Figures 19 (Runs 1, 4, and 5), 20 (scale expansion of Figure 19), 21 (Runs 6, 7, and 8), and 22 (scale expansion of Figure 21) show effects of continued sequential irradiation of the same sample followed by photomultiplier analysis. In all cases, the control remains flat and constant, suggesting that the observable decay is due only to direct irradiation of the PMMA sample.

Experimental conditions and apparatus design were such that only a small portion of the actual decay curve for irradiated PMMA could be detected. Because of light leaks in the system, readings could not be taken until 15 seconds after actual sample irradiation and lamp shutoff. Furthermore, because of the particular experimental setup and the limited scope of the effort, it was not possible to examine the spectral distribution of light emitted from the preirradiated samples Despite these deficiencies, quantitative information was obtained related to the irradiation of PMMA and subsequent analysis by chemiluminescence techniques

Graphical analysis of the decay curves for irradiation of PMMA under nitrogen (Figures 15 and 17) suggests an apparent fit to a semilogarithmic linear plot (first order decay reaction) of counts per second (intensity) versus time (Figure 23) Experimental Runs 1, 2, and 6 (each 10-second individual exposure times) are approximately equivalent and fall along almost the same line Run 3 (20 seconds individual exposure time or a cumulative exposure time of 40 seconds) resulted in a very high initial counts-per-second intensity reading while Runs 4 and 5 produced lower initial counts-per-second intensity values Attempts to rationalize these results on a constant counts-per-second intensity reading taken at 6 seconds (vertical line indicating approximately 50 percent relative decay rate in Figure 23) versus cumulative exposure times (cumulative exposure time = exposure time of Run 1 + Run 2 + Run 3 + etc) for Runs 1 through 6 did not produce a meaningful correlation (Figure 24). Runs 1, 2, and 7 (individual exposure times of 10 seconds) remained essentially constant at counts-per-second values between 600 and 700, while Run 3 increased in intensity and Runs 4 and 5 showed a dramatic decrease in counts-per-second readings (300 to 950; readings taken from 6-second vertical line of Figure 23). It is possible that during irradiation of the PMMA several intermediates are being formed or destroyed and/or that the observed photostimulated emission is dose or intensity sensitive and is responsible for the noncorrelatable results shown in Figure 24. These findings will require more experimental evidence for confirmation and interpretation of results in order to distinguish between photophysical and photochemical reaction pathways in the irradiated PMMA sample.

Graphical analysis of the decay curves for irradiated PMMA in air (Figures 21 and 22) (first order decay) produced linear semilogarithmic plots (Figure 25) similar to those observed for identical experiments carried out under nitrogen. One notable difference between the samples irradiated in nitrogen and those irradiated in air is that the initial chemiluminescence intensity readings are somewhat higher under nitrogen (values range from 800 to 2000 counts-per-second).

A plot of relative cps readings taken at a constant relative decay rate of 6 seconds (points taken off of Figure 25) against cumulative exposure time for each run showed a definite trend toward decreasing relative intensity between runs (Figure 26) It appears that an intermediate or photophysical process is being destroyed or deactivated with each cumulative and subsequent irradiation exposure in a predictable manner The decrease in air versus nitrogen initial intensity readings and the predictable decline of intensity with cumulative exposure indicates that the photochemical/ photophysical reactions are oxygen sensitive Filter experiments indicate that these results are only produced through 254 nm UV-irradiation wavelengths in this material Other experiments[7] have indicated that the quantum efficiency of UV degradation in some materials (e.g , RTV 615) is independent of wavelength over the range 230-320 nm.
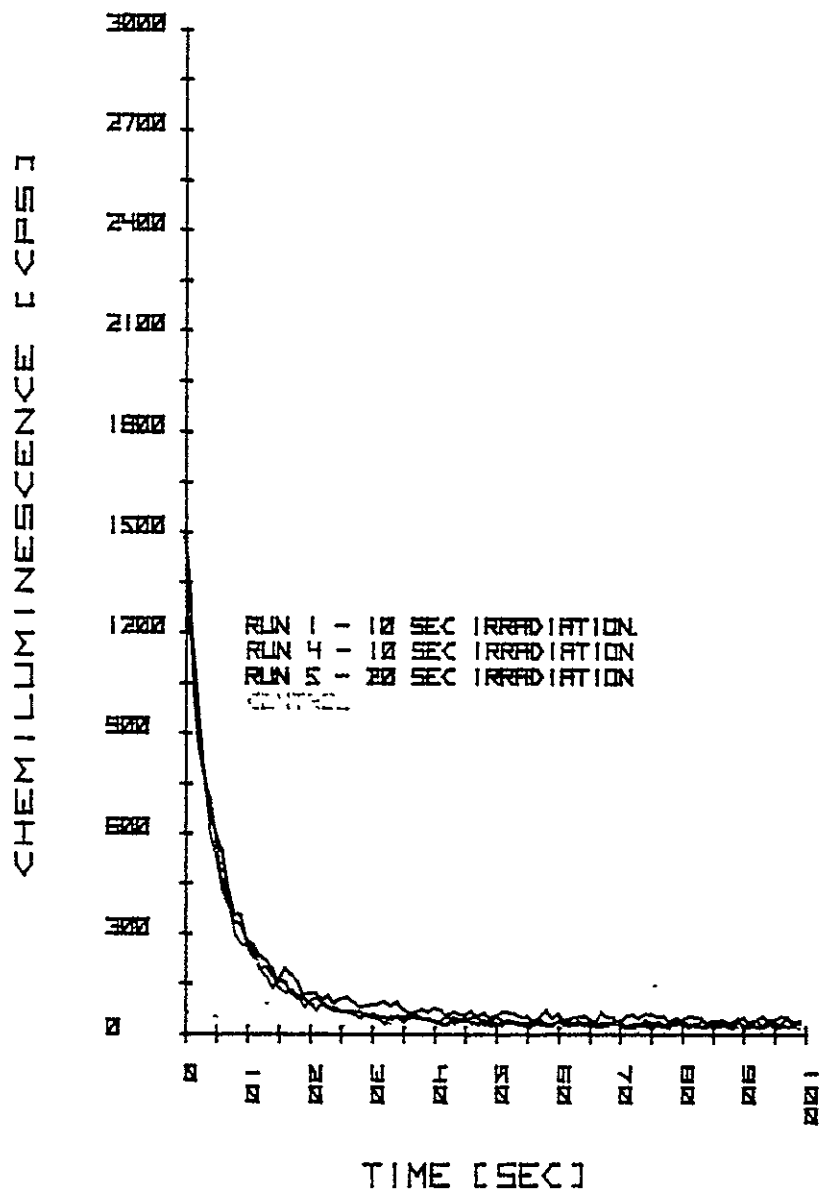
FIGURE 19. INTENSITY PLOT OF CPS VERSUS TIME FOR
PMMA IRRADIATION IN AIR

The individual runs had 10, 10, and 20 seconds
exposure time (cumulative exposure time =
40 seconds).

31
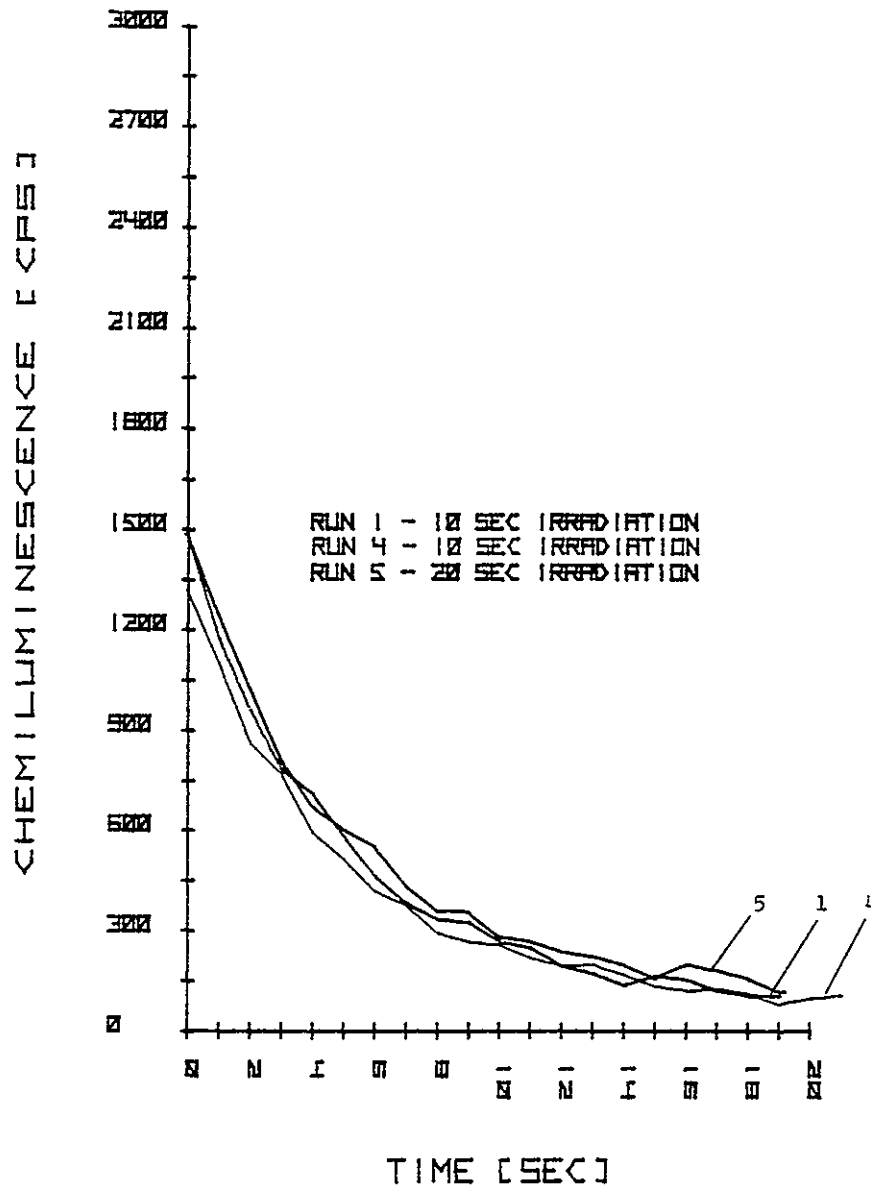
FIGURE 20. SCALE EXPANSION OF FIGURE 19

32
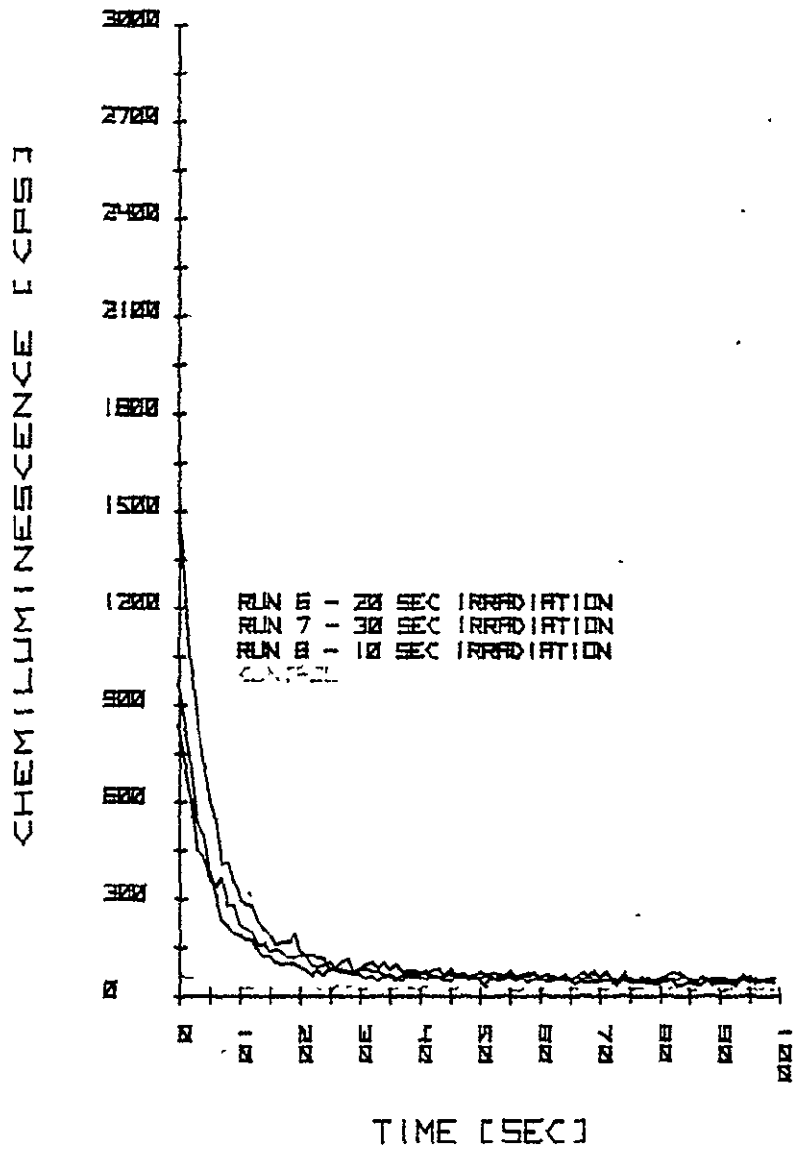
FIGURE 21. INTENSITY PLOT OF CPS VERSUS TIME FOR PMMA
IRRADIATION IN AIR

The individual runs (6, 7, and 8) had 20, 30, and 10
seconds exposure time (cumulative exposure time =
100 seconds).

33
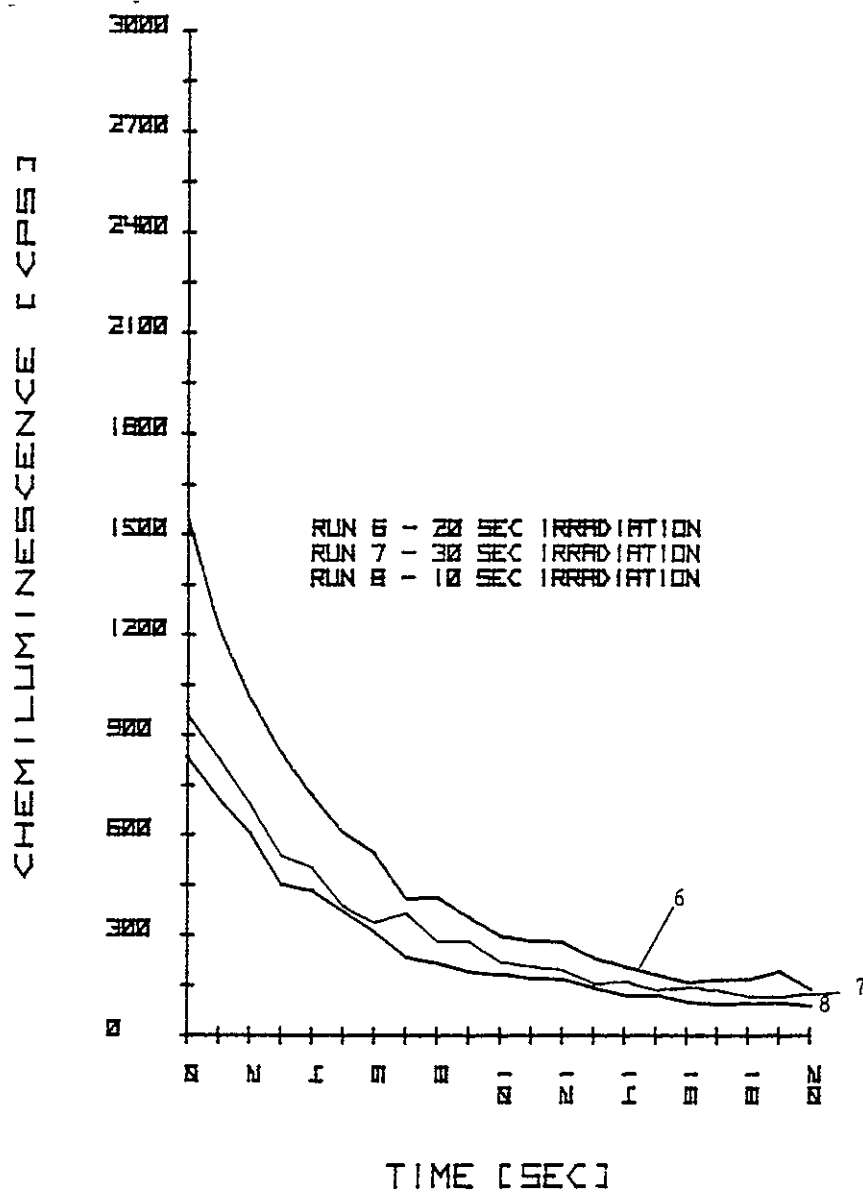
FIGURE 22. SCALE EXPANSION OF FIGURE 21

34
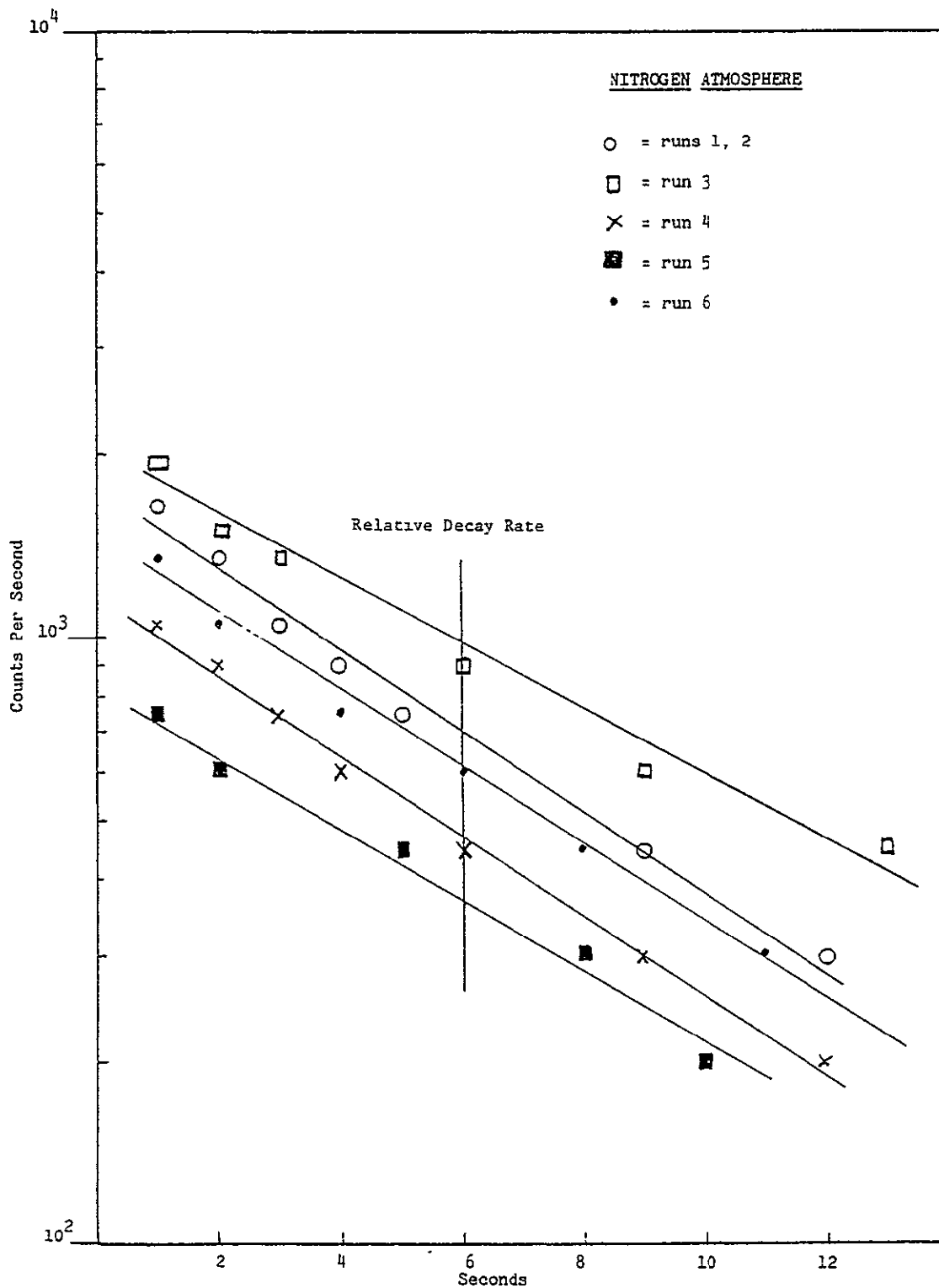
FIGURE 23. SEMILOGARITHMIC PLOT OF INTENSITY (CPS) VERSUS TIME (SECONDS) FOR RUNS 1 THROUGH 6 (IRRADIATION OF PMMA IN NITROGEN)

35
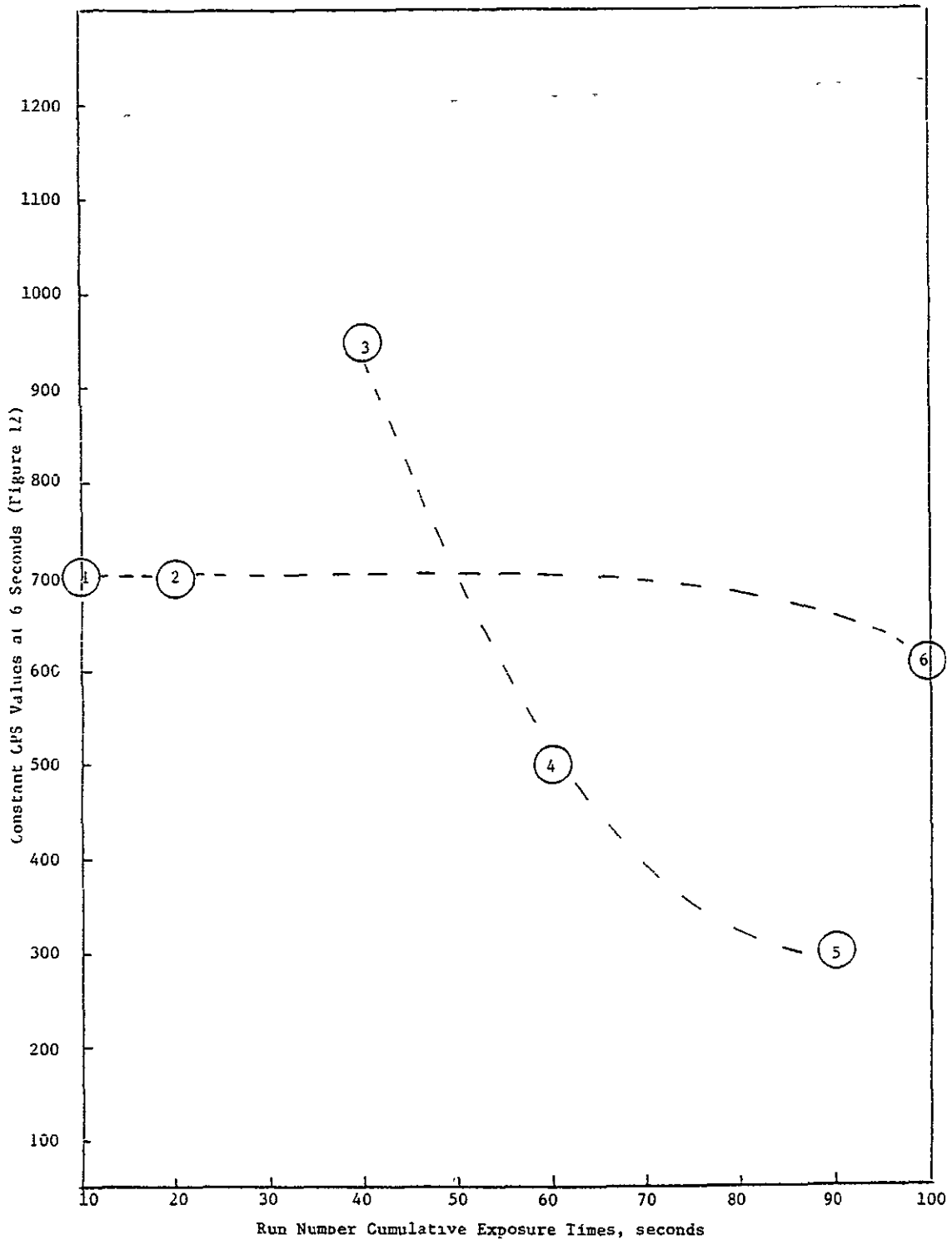
FIGURE 24. PLOT OF CONSTANT CPS INTENSITY READING TAKEN AT 6
SECONDS (VERTICAL LINE INDICATING APPROXIMATELY
50 PERCENT RELATIVE DECAY RATE IN FIGURE 23) VERSUS
CUMULATIVE EXPOSURE TIME FOR RUNS 1 THROUGH 6

36
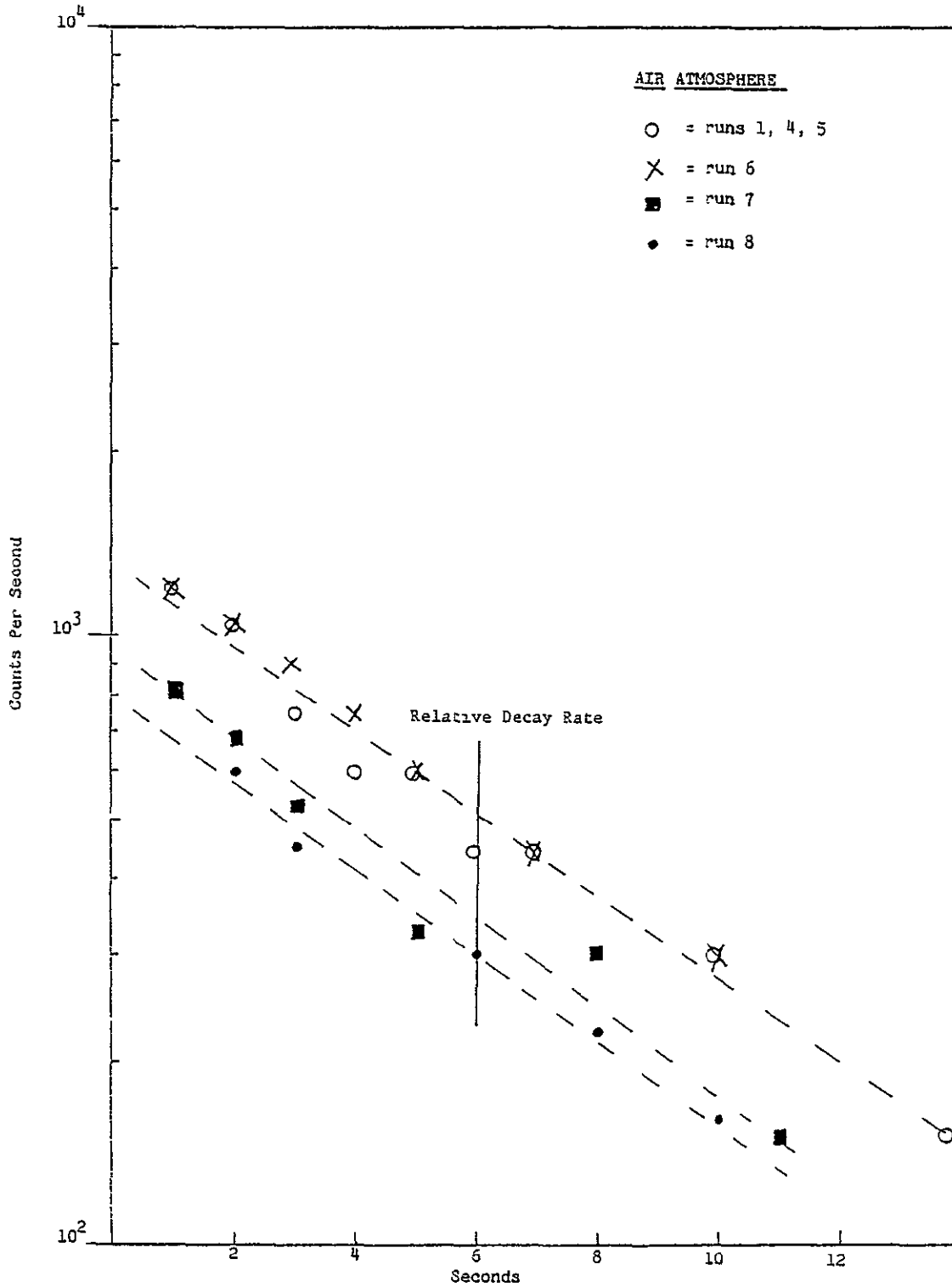
FIGURE 25. SEMILOGARITHMIC PLOT OF INTENSITY (CPS) VERSUS
TIME (SECONDS) IN RUNS 1, 4, 5, 6, 7, AND 8 (IRRADIATION
OF PMMA IN AIR)

37
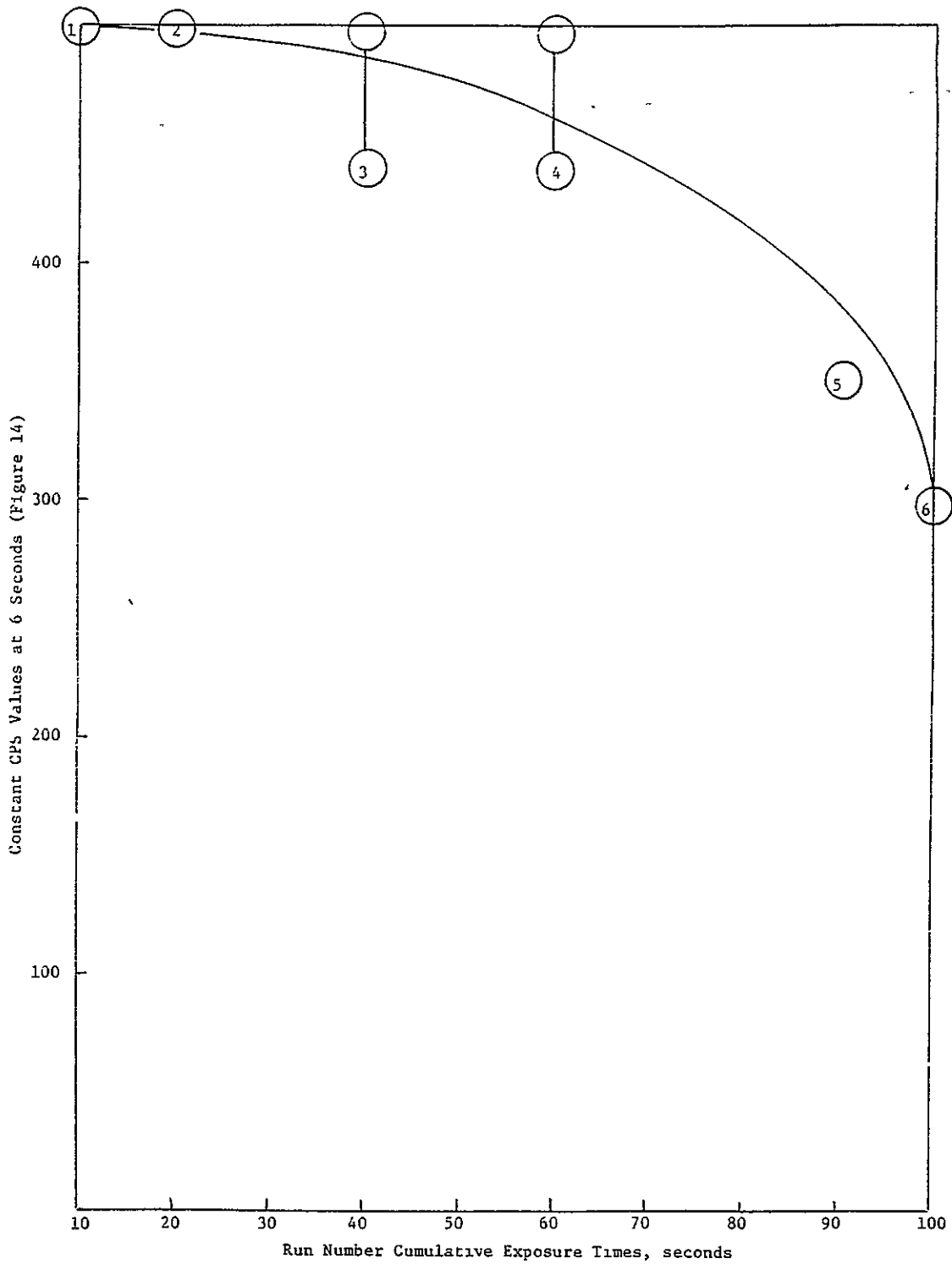
FIGURE 26. PLOT OF CONSTANT CPS INTENSITY READINGS
TAKEN AT 6 SECONDS (VERTICAL LINE INDICATING
APPROXIMATELY 50 PERCENT RELATIVE DECAY
RATE IN FIGURE 25) VERSUS CUMULATIVE EXPOSURE
TIMES FOR RUNS 1, 4, 5, 6, 7, AND 8

38

Conclusions and Recommendations — Chemiluminescense

Chemiluminescence analysis techniques have been used in this study to examine photostimulated emissions of pure PMMA samples. These observable first–order–decay emissions are oxygen sensitive and might be related to some small change in long range order or polymer-structure modifications associated with absorption of 254 nm wavelength energies. This analysis technique is apparently very sensitive and might be used to study polymer photophysical processes or to detect small changes in polymer structure, even after very short irradiation exposure times. At this time, it can be said that small but measurable changes in the photomultipher output signal were observed in the Battelle work under experimental conditions very similar to those reported by Dr. Gupta in his research involving irradiation of pure PMMA samples. Dr. Gupta has observed formation of a short–lived intermediate (FTIR confirmation) after irradiation of PMMA with a Hg light source for 1 to 10 seconds' exposure time.

In future studies concerned with the long-term characterization of polymeric materials, under actual or accelerated testing conditions, it will be necessary to correlate chemiluminescence analysis studies with other techniques such as ESR, GPC, flash photolysis, and mechanical testing. Several modifications to the present chemiluminescence equipment would also be desirable in measurements intended for this application. These would include constant temperature control, absolute atmosphere variability, irradiation, thermal and mechanical stress capability, and means for spectral analysis of emitted light before photomultiplier tube signal detection. With these modifications, it should be possible to begin service life evaluation of field samples with a much higher degree of sensitivity than is currently realized for other analytical equipment and techniques. With a calibrated (calibration in this sense means that the instrument will respond accurately and reproducibly to a control sample over extended periods of time) chemiluminescence apparatus, it should be possible to observe spectral shifts or changes in a decay curve as a function of field time and stress

These experiments have demonstrated that chemiluminescence can be used to observe small changes in PMMA standards under controlled irradiation conditions It is recommended that this work be extended to investigate more complex polymeric systems such as those associated with present and proposed photovoltaic module designs. The implementation of more advanced studies of the usefulness of chemiluminescence measurements in lifetime-prediction studies of photovoltaic modules will require an apparatus incorporating the capabilities outlined above and evaluations in conjunction with other characterization techniques

Electrical Noise Measurements

Background

One of the potential degradative processes in photovoltaic modules and arrays in terrestrial environments is corrosive attack of the contact metallization and the interconnects. The primary agents for this attack are expected to be water and oxygen. Attack by substances evolving from the encapsulants is also possible.' Mechanical stress can be a contributing factor, especially in regions where interconnects and contact metallization are bonded.

A major manifestation of degradation of this type is an increase in the series resistance of the device or module Unfortunately, the sensitivity and precision associated with series-resistance determinations for photovoltaic devices and modules is not high in current practice High sensitivity and

precision are critically important characteristics in measurements for life prediction studies. It is desirable, then, to identify and evaluate techniques that promise improvements over standard series-resistance determinations.

Electrical current noise, also known as "1/f" noise, has been found in many cases to be highly sensitive to defects -- including failing electrical contacts -- in electronic components and devices.[8] Noise power variations as great as several orders of magnitude have been observed between normal and abnormal units.[9] The use of low-frequency noise measurements as a screening test for identifying short-lived and long-lived passive and active electrical devices has received sporadic attention during the past two decades.[9-11]

A natural extension of this effort would be the use of such measurements to track the degradation of electrical devices such as solar cells. This concept is further encouraged by several studies which have shown that 1/f noise measurements can be used to assess the quality of ohmic contacts to semiconductors and which have established both analytically and experimentally that these measurements are *more* sensitive than first-order characteristics (e. g., I-V characteristics) to changes in contact properties, including contact resistance and "patchiness" of contacts.[12-14] However, no data directly applicable to p-n junction photovoltaic devices and modules have been found in an extensive literature search and in discussions with experts in the field and with equipment manufacturers. Experimental evaluation of the applicability and usefulness of electrical noise measurements in studying the degradation of metallization and contact regions was therefore recommended.

The objective of these experiments was to determine the sensitivity of electrical current noise in p-n junction photovoltaic cells and in modules using such devices to degradative changes in the cell contact metallization. These degradative changes may by associated with corrosive attack of the contact or interconnect metallization or with other contact debonding mechanisms.

Experimental Plan and Equipment

To establish the applicability of electrical noise measurement to studies of contact metallization degradation, two categories of experiments were judged desirable. The first type of experiment was aimed at establishing that the low-frequency noise characteristics of photovoltaic cells are of the current-noise of 1/f type, i. e., that the noise power exhibits a current-density dependence and spectral distribution in conformance with the expression

$$P_n = \frac{kI^2\Delta f}{f},$$

where P_n is the noise power in the measurement band width Δf, I is the current density, k is a constant, and f is the frequency at which the measurement is made or centered. The major concern here was that other types of noise (e. g., generation-recombination noise and "pop-corn" noise[15]) might be of sufficient magnitude at low frequencies in these devices to prevent identification and measurement of the 1/f type noise. This point is important because (1) the 1/f noise is the type that appears to be most sensitive to, and directly correlatable with, contact resistance changes, and (2) the low-frequency noise characteristics of photovoltaic devices have not been previously established. Experiments to establish the degree of conformance of solar cell, low-frequency noise characteristics to the above expression were conducted as part of this evaluation

If l/f noise is manifested, a second category of experiments is desirable. These experiments would be focused on determining the correlation of cell series–resistance values (and changes in those values) with l/f noise levels If a correlation is established, a comparison between the sensitivity of detecting series–resistance changes by noise level measurements and conventional methods becomes important Some experiments of these types were also conducted as part of this evaluation

The basic experimental arrangement used in these experiments is illustrated in block diagram form in Figure 27. The key element of this arrangement is a Hewlett–Packard model 5420A Digital Signal Analyzer, which permits measurement and analysis of the device noise characteristics A bias circuit was used to control current flow through the device during the measurement Both the current flow through the device and the voltage drop across it were measured with a HP model 3465A digital multimeter The noise signal was amplified by an Ectron model 418 low–noise broad–band amplifier prior to being fed to the signal analyzer. The experimental setup also incorporated a standard test diode, which could be switched into the circuit in place of the photo-voltaic device under test for calibration and operational checking purposes.

All measurements were made with the photovoltaic device in the dark (in a light–tight container) and with the device mounted on a water–cooled copper platen to maintain constant and controlled temperature conditions during all measurements. Cell temperature was monitored continuously Periodic measurements of the noise associated with the amplifier (input shorted) and the noise associated with the circuit with no current flowing through the device were made to ensure that the noise characteristics measured were attributable to the photovoltaic device A typical amplifier noise plot (noise power in dBm versus frequency) over the band 200 Hz–25 KHz is shown in Figure 28.

The photovoltaic cells used in these experiments had screen–printed silver front contacts and were of a type that previous testing had shown tended to develop contact resistance problems upon high humidity and/or thermal cycling stress. These cells were selected for these studies because of this characteristic

Measurements and Results

Spectral Distribution of Electrical Noise in Photovoltaic Devices. Figure 29 is a plot of noise power versus frequency over a 200 Hz–25 KHz range for a typical 2–inch–diameter silicon cell with screen–printed silver contact metallization. The noise power density of the cells was typically flat from about 10 Hz out to about 4 KHz. It slowly decreased over the remainder of the spectral range shown, and was generally in the range of –80 to –90 dBm at the current density indicated (29.6 mA/cm^2 which is of the order of the short–circuit current of these cells). This behavior was similar to that observed in the presence of generation–recombination noise, and indicated that, for the purposes of these experiments, the major part of this spectrum (i e., the higher frequencies) was not of interest and that generation–recombination noise posed significant problems in these measurements. The thermal noise power per unit band width associated with the effective resistance of the circuit at ambient temperature was calculated and found to be of the order of 10^{-19} watt or –160 dBm. This was well below the measured noise power level even under conditions where no current flowed through the circuit.

A typical plot of the spectral distribution of the measured noise level with no current flowing in the circuit is shown in Figure 30 over the 1–100 Hz band. In general, the no–current noise levels were essentially identical to the amplifier noise over the entire spectral region of 0–25 KHz.

41
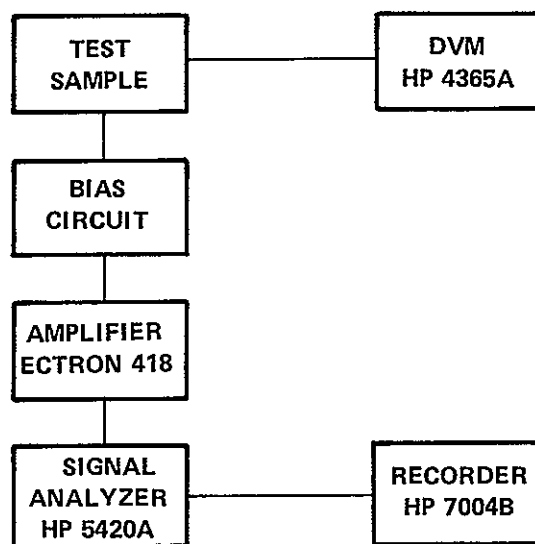
FIGURE 27. BLOCK DIAGRAM OF NOISE MEASUREMENT EXPERIMENT`
EQUIPMENT ARRANGEMENT
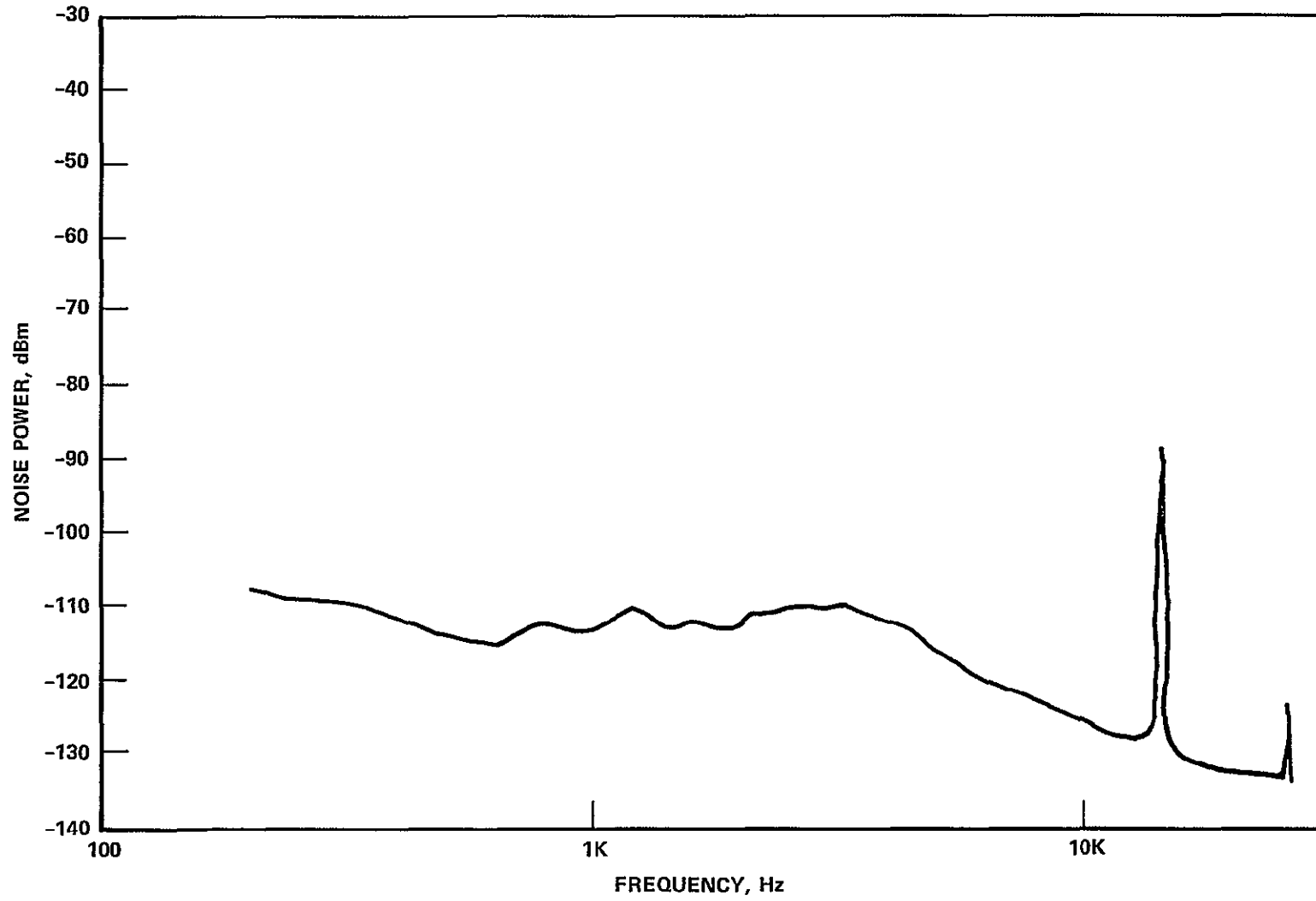
FIGURE 28. ECTRON AMPLIFIER NOISE PLOT OVER THE RANGE
200 Hz TO 25kHz; BANDWIDTH 100 Hz

FIGURE 29. NOISE CHARACTERISTIC OF CELL #411 OVER THE RANGE
200 Hz – 25 kHz; BANDWIDTH 100 Hz
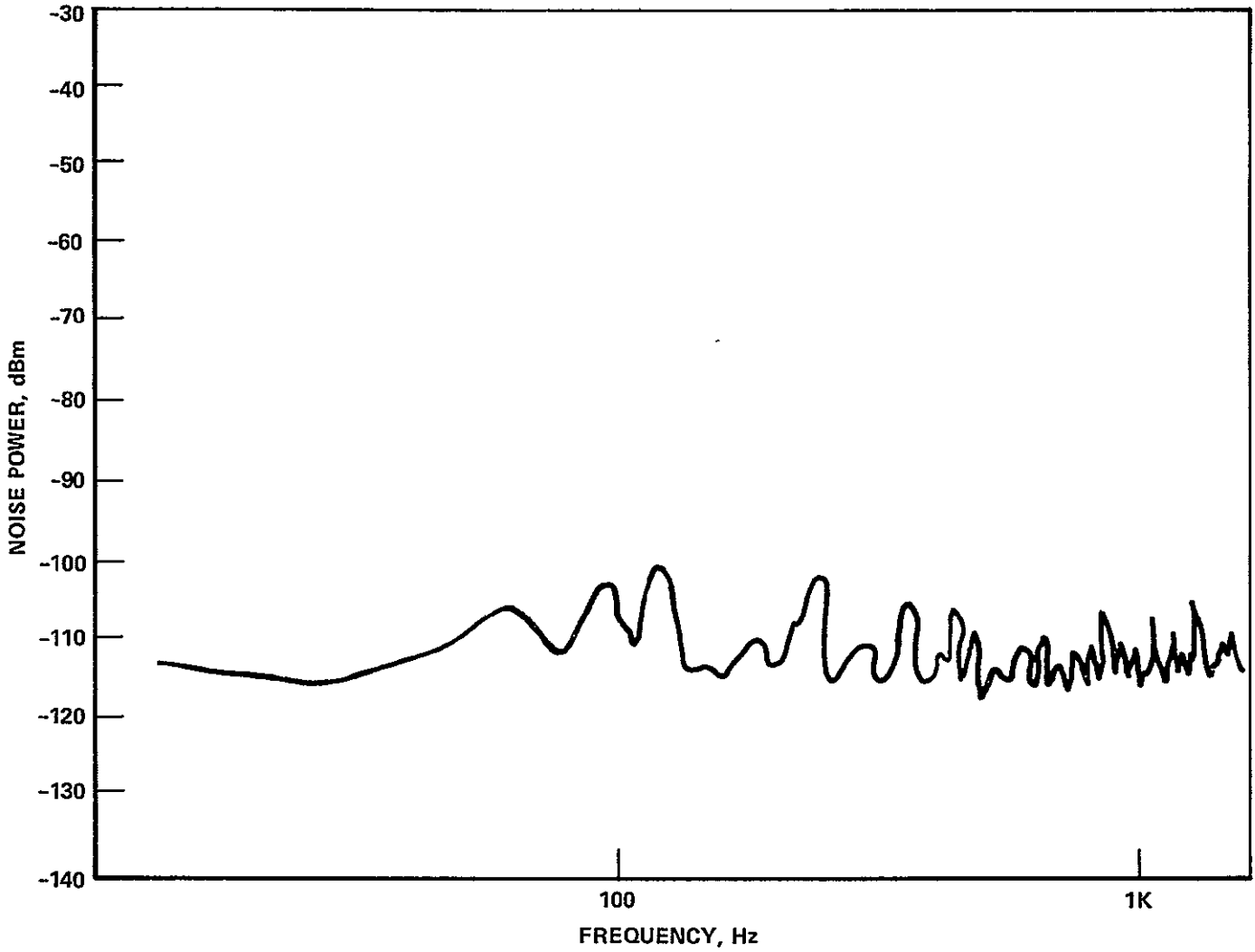
FIGURE 30. NOISE CHARACTERISTICS OF CELL #411 WITH NO CURRENT
FLOWING FOR THE SPECTRAL RANGE 1 – 1000 Hz;
BANDWIDTH 6 Hz

45

The noise level under no-current conditions was measured for all of the cells used in these experiments and was reasonably consistent, as would be anticipated. Noise levels under these conditions were in the range of –90 to –95 dBm at 0 1 Hz They flattened out at about –110 to –120 dBm at 10 Hz and remained at this level up to about 3–5 KHz, after which they dropped off gradually to –130 to –140 dBm at 25 KHz, which was the high-frequency limit of the equipment. These noise levels were considerably above the calculated thermal noise level, indicating that other noise-sources were present and dominated the thermal noise in this spectral region.

Plots of noise power versus frequency over the range 0–1000 Hz are shown in Figure 31 for several cells The current density for these curves was 29.6 mA/cm^2. Even over this range, the noise power was essentially insensitive to frequency except for frequencies of about 1 Hz or less. For this reason, the attempts to analyze the noise characteristics of these devices and to establish correlations with series–resistance determinations were focused between 0 and 2 Hz

The Effect of Current Density on Electrical Noise in Photovoltaic Devices. Figure 32 illustrates the current-density dependence of the noise power density for several cells at a fixed frequency of 0.1 Hz over the current-density range 0–45 mA/cm^2 Figure 33 shows a similar plot for a frequency of 1 Hz and Figure 34 shows the noise power in the 0–2 Hz band as a function of current density

At the lower current densities (0–20 mA/cm^2) in Figures 32 and 33, the noise characteristics of the cells were generally very similar (as evidenced by the close grouping of the data points in these figures in this current density range) and generally appeared to vary more slowly than I^2 in this range (in fact usually sublinearly). At current densities above the 20–25 mA/cm^2 level, the differences in noise characteristics between individual cells appeared to be more clearly delineated and there was considerably more spread in the data points. In the higher current density ranges, the variation of noise power (at the fixed frequency points given) with current density appeared to be significantly higher than an I^2 dependence in most cases, although one cell did continue to show a sublinear dependence in this range. It can also be seen that in many cases the cell's noise characteristics did not vary in a consistent and continuous manner as a function of current density The broader band data (0–2 Hz) shows in Figure 34 exhibited similar inconsistencies in current dependence with a fairly uniform spread amongst the different cells throughout the entire range of current densities evaluated (i. e., the transition in the current density range 20–30 mA/cm^2 was not apparent in the broader band data). The 0–2 Hz band included a portion of the spectral range in which the cell noise characteristics appeared to be frequency dependent.

In addition to the behavior illustrated in Figures 33 and 34, many of the cells exhibited fluctuating instabilities during testing. These instabilities were of a bistable nature, in that the current flow through the cell at constant cell bias fluctuated between two distinct levels with varying periods between fluctuations. The fluctuations were as high as 5 to 10 percent of the bias current level and were most prominent at current densities corresponding to the maximum power point current (AMI) or greater. This type of behavior is typical of so-called "pop-corn" noise or burst noise[15], which is observed in other types of semiconductor devices and is generally attributed to imperfect semiconductor surface conditions incurred during wafer processing Since the cells used in these experiments were developed around a low-cost concept that minimizes processing and handling (including surface preparation and treatment), it is conceivable that appropriate conditions for generation of burst noise might be present Another possible explanation for the observed behavior is that there is localized making and breaking of the electrical contact between the contact grid and the semiconductor surface due to heating and other current flow phenomena at the higher current densities. This behavior would result in fluctuations of the
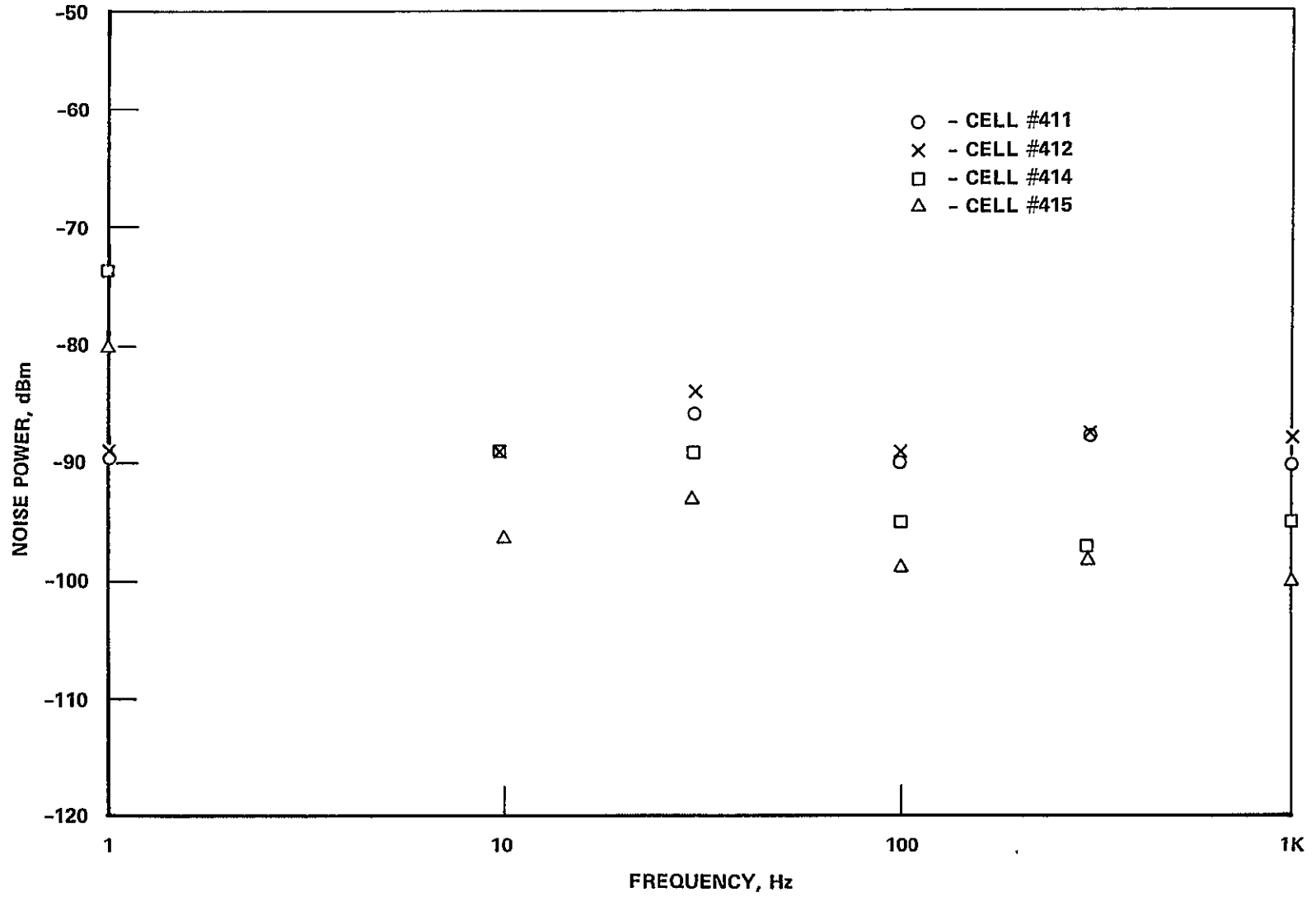
FIGURE 31. SPECTRAL DISTRIBUTION OF NOISE POWER FOR CELL NOS.
411, 412, 414, AND 415 FOR THE RANGE 1 – 1000 Hz;
BANDWIDTH 6 Hz
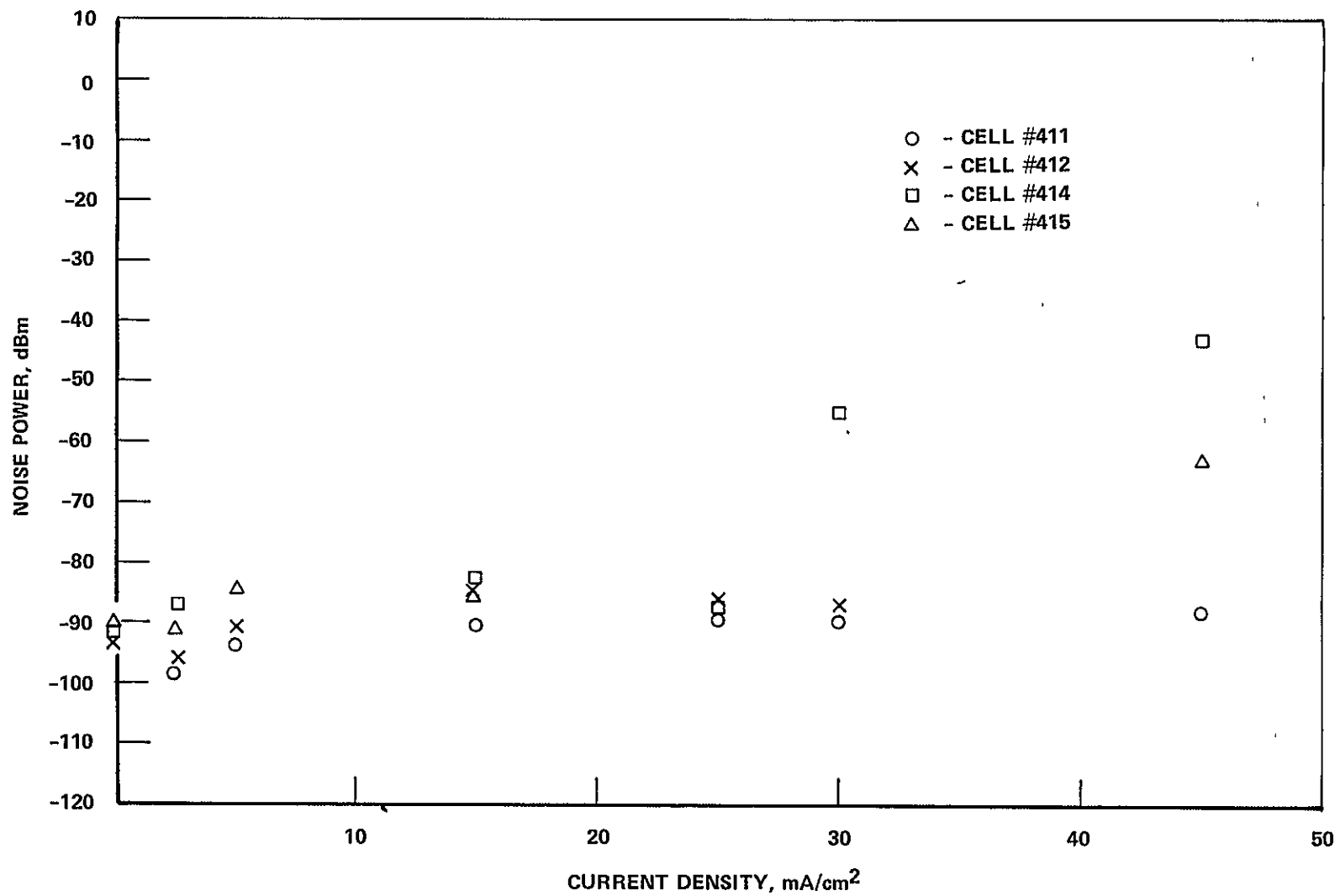
FIGURE 32. CURRENT DENSITY DEPENDENCE OF NOISE POWER FOR CELL
NOS. 411, 412, 414, AND 415, CENTER FREQUENCY 0.1 Hz;
BANDWIDTH 8 mHz
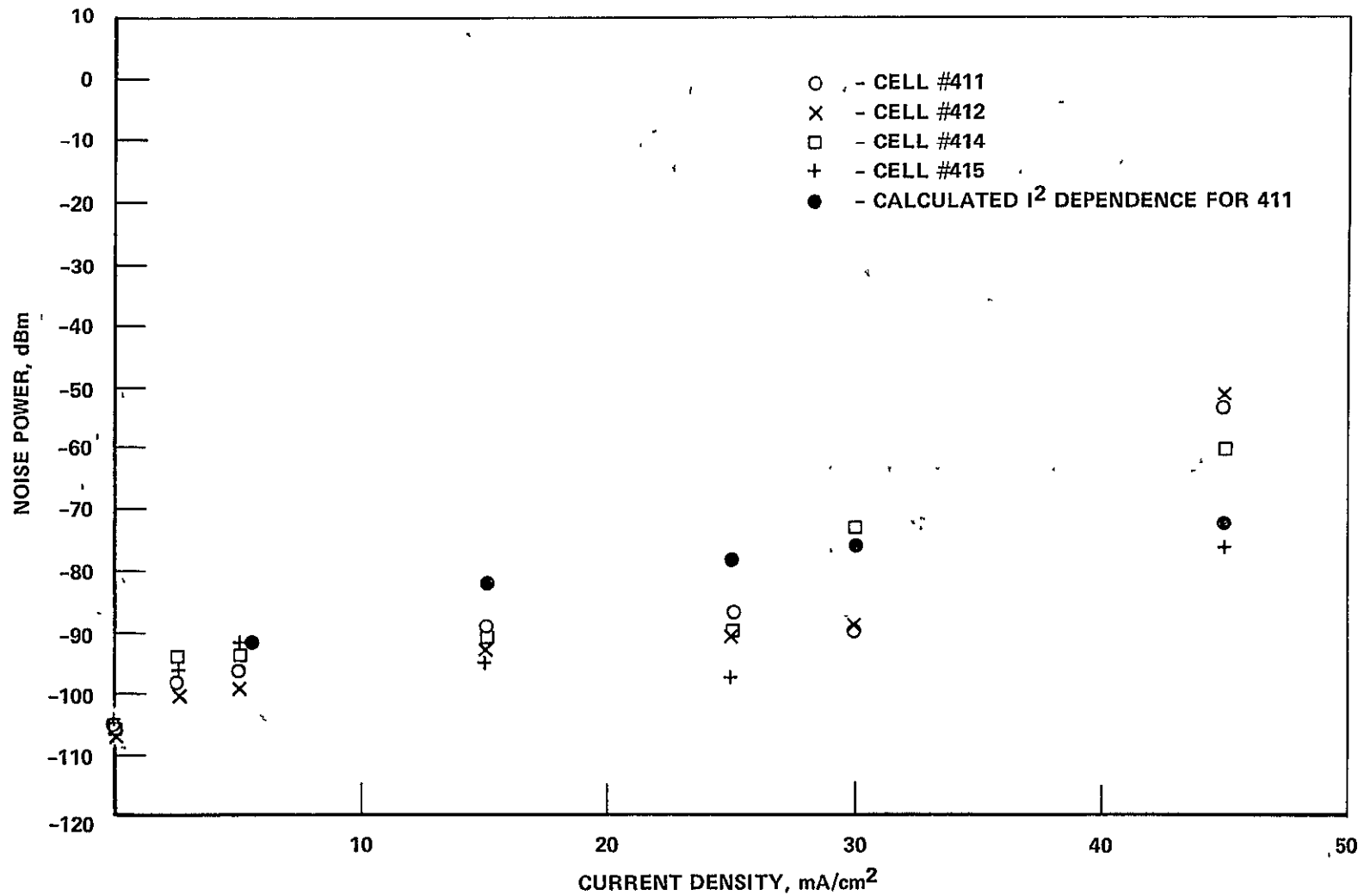
FIGURE 33. CURRENT DENSITY DEPENDENCE OF NOISE POWER FOR CELL NOS. 411, 412, 414, 415. CENTER FREQUENCY 1 Hz, BANDWIDTH 8 mHz

The filled dots ( ) indicate anticipated I^2 type variation for cell #411, the open dots ( ) are measured behavior for this cell.

49
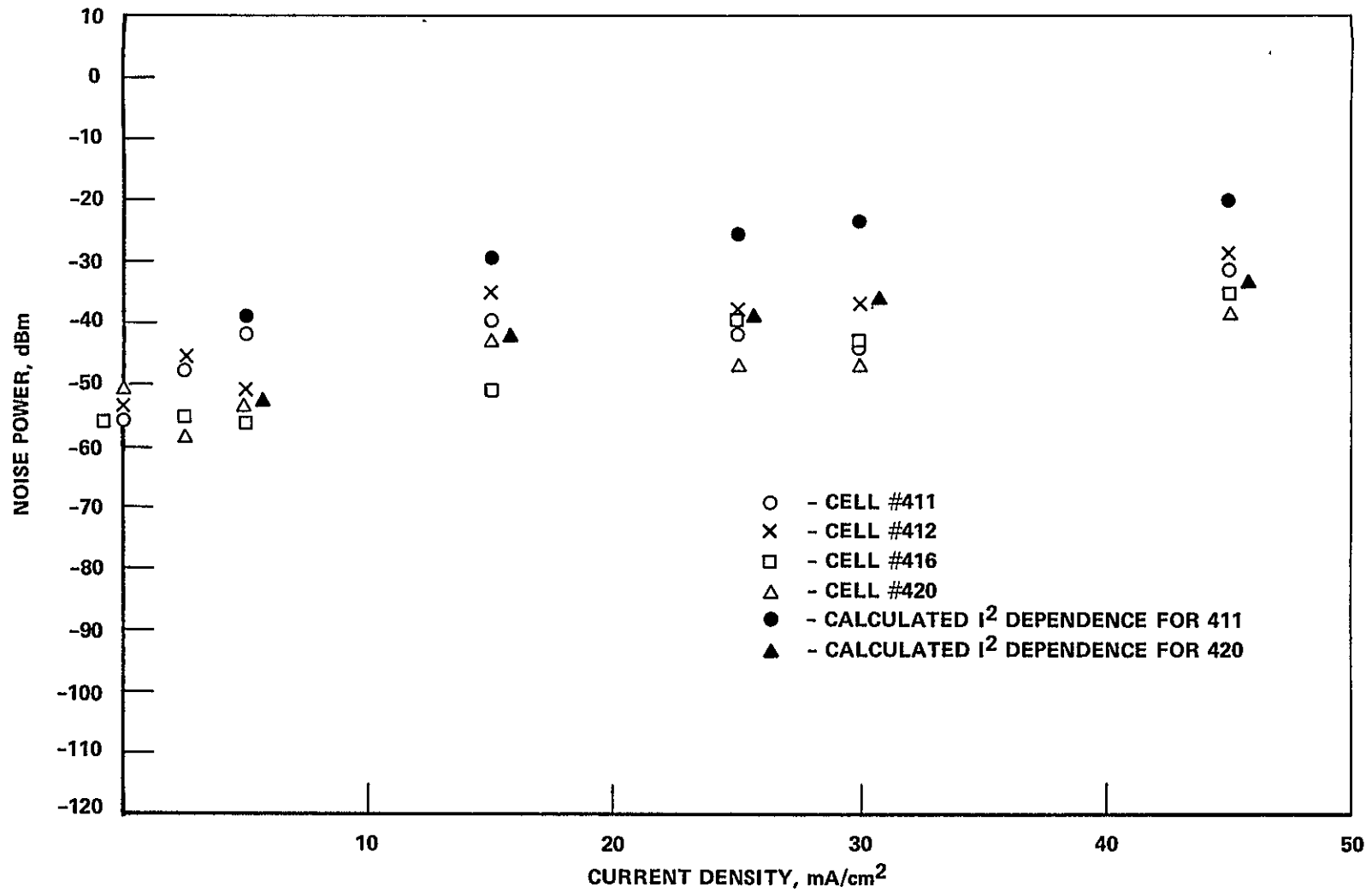
FIGURE 34. CURRENT DENSITY DEPENDENCE OF NOISE POWER FOR CELL NOS.
411, 412, 416, AND 420

Data shown are for total power in the bandwidth 0 — 2 Hz. The darkened
triangles ( ) represent the anticipated envelope for these cells assuming an
1^2 dependence.

50

effective contact area, and hence the series resistance of the cell, thereby causing the observed effect. Either of these effects (i e., surface condition burst noise or contact area fluctuations) could be peculiar to this specific cell type. Sufficient testing to establish the existence or non-existence of this behavior in other cell types was not possible within the scope and time frame of this effort

Correlation Between Series-Resistance Values Derived from I-V Characteristics and Low-Frequency Noise Measurements. Despite the inability to establish appropriate current-density dependence for classical current (1/f) noise behavior in the photovoltaic cells, attempts were made to correlate low-frequency noise levels with series-resistance values derived from current-voltage characteristics using the standard technique of Wolf and Rauschenbach.[16] Comparisons of the electrical noise of cells having different values of series-resistances were made, and comparisons of before-and-after stress noise levels were made for cells that were exposed to high humidity

Figure 35 shows a plot of noise power density (0-2 Hz band) versus derived series resistance for a set of unstressed cells. The series-resistance values for the cells used in this experiment were in the range of 0.05-0.16 ohm. There appears to be no obvious trend or correlation from the data in Figure 35. This would be the case if the cells' series resistance is not dominated by contact resistance or, obviously, if the electrical noise is not primarily 1/f noise and/or can not be correlated with series resistance as calculated from I-V characteristics

The degree of uncertainty in the derived series-resistance value is also a consideration. Assessment of the true correlation would require an independent determination of the contact resistance component of the series resistance This is a difficult task to perform with any precision on these devices An alternative is to stress the cells to produce changes in the contact resistance and attempt to correlate changes in the electrical noise level with apparent changes in series resistance due to the contact resistance changes. A limited experiment of this type was performed, however, difficulties with cell damage and equipment malfunction prohibited collection of extensive data in this area

Several cells were characterized (both I-V and noise characteristics measured) and subsequently subjected to high-humidity conditions (100 percent RH @ 30 C) for approximately 48 hours. Their I-V and noise characteristics were then remeasured with the objective of correlating changes in the resistance with changes in the noise. The pre-stress, low-frequency (0-2 Hz) noise power of all of the cells used in this experiment was in the range of -74 to -78 dBm, and their pre-stress series-resistance values as derived from the I-V characteristics were in the range 0.07 to 0.12 ohm. Exposure to the high-humidity stress resulted in widely varying changes in the series resistance of the cells. Most of the cells showed increases in series resistance ranging from 5 percent to 65 percent. One cell, however, exhibited a *decrease* of about 26 percent. All cells experienced a substantial and essentially identical increase in noise power, with the post-stress noise power values of all of them falling in the range of -45 to -52 dBm.

It is apparent that the high-humidity stressing had a significant effect on the mechanism that is responsible for the generation of the low-frequency electrical noise, since the noise power increased by approximately 2-3 orders of magnitude in all cases. However, it is also apparent that the changes ·in the cells' noise characteristics do not correlate with the changes in the series resistance of the cells as determined from their I-V characteristics. Whether or not the observed changes correlate with some other mode of degradation cannot be determined from these data.

51
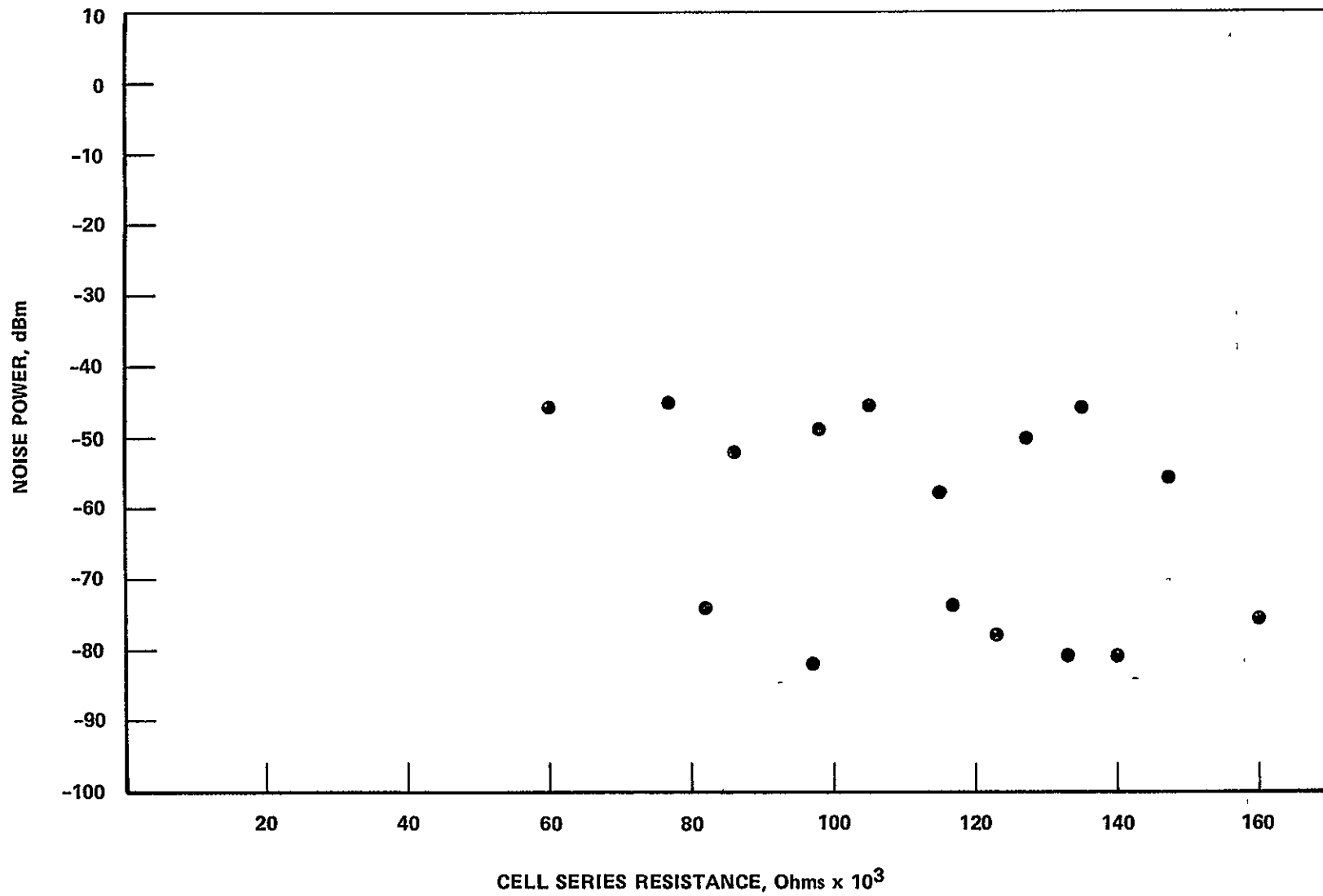
FIGURE 35. NOISE POWER VS I-V CHARACTERISTIC DERIVED SERIES
RESISTANCE FOR A SET OF UNSTRESSED CELLS

Conclusions and Recommendations — Electrical Noise Measurements

It was found that generation–recombination noise and possibly burst noise or other types of low–frequency noise are present in significant magnitudes in the particular type of photovoltaic cells used in these experiments. These types of noise make it difficult to distinguish the 1/f noise associated with contact degradation and tend to obscure the correlation with cell series resistance. In studies of the reliability of transparent–conductive oxide semiconductor type cells[17], other investigators have experienced similar difficulty in separating 1/f noise from the generation–recombination noise Clearly means of separating the various contributions to low–frequency noise in these photovoltaic devices should be determined in future studies.

The mechanism responsible for the dominant low–frequency noise in these devices appears to be sensitive to high humidity Experiments to determine if this effect can be correlated with some other degradation mode should be conducted. Experiments to establish whether or not other types of cells exhibit noise characteristics similar to those of the cells used in these experiments are also recommended

REFERENCES

(1) Jet Propulsion Laboratory, "Project Quarterly Report–4 for the Period January 1977–March 1977", Low–Cost Silicon Array Project, Report No. ERDA/JPL–1012–77/3

(2) Jet Propulsion Laboratory, *9th Project Integration Meeting, Low–Cost Silicon Solar Array Project (Proceedings)*, JPL Report No. 5101–67 (April 11–12, 1978)

(3) Thomas, R. E., and Carmichael, D. C., "Terrestrial Service Environments for Selected Geographic Locations", Battelle's Columbus Laboratories Report No. ERDA/JPL–954328–7615 (June 24, 1976).

(4) Noel, G. T., et al., "Measurement Techniques and Instruments Suitable for Life–Prediction Testing of Photovoltaic Arrays", Interim Report on JPL Contract No. 954328, Report No. DOE/JPL–954328–78/1, January 15, 1978.

(5) Howes, V. R., Wear, **39**, 123 (1976).

(6) Tomandl, G., J. Non–Cryst. Solids, **19**, 105 (1975)

(7) Gupta, A., "Effect of Photodegradation on Chemical Structure and Surface Characteristics of Silicone Pottants Used in Solar Cell Modules", LSA Project Report 5101–79 (August 18, 1979).

(8) Van der Ziel, A., *Fluctuation Phenomena in Semiconductors*, Academic Press, Inc. (1959).

(9) Gupta, M., Proc. IEEE, **63** (7), 1006 (July 1975).

(10) Curtis, J. G., International Electronics, p. 10–13 (May 1962).

(11) Van der Ziel, A. and Tong, H., Electronics, p. 95–97 (November 28, 1966).

(12) Rolland, M., et al., Solid State Electronics, **20**, 323–331 (1977).

(13) Vandamme, L K. J. and Tijburg, R. P., Jour. Appl. Phys., **47** (5), 2056–2058 (May 1976).

(14) Nougier, J. P. and Rolland, M., Solid State Electronics, **16**, 1399–1405 (1973).

(15) Soderquist, D., "Minimization of Noise in Operational Amplifier Applications", Precision Monolithics, Inc., Application Note No. AN–15.

(16) Wolf, M. and Rauschenbach, H., Adv. Energy Conv., **3**, 455 (1963).

(17) Dubow, J., Univ of Colorado, private communication.

APPENDIX A

SUMMARY OF PHASE I RESULTS

APPENDIX A

SUMMARY OF PHASE I RESULTS

The objective of the first phase of the study was to evaluate instruments and techniques for the quantitative measurement of degradation-related changes in the properties of photovoltaic materials and arrays. Emphasis was placed on precursors to the failure of such arrays. The results of this phase were presented in an interim report (Report No DOE/JPL-954328-78/1) A summary of the results and recommendations presented in that report are repeated here

The study focused on techniques and instruments that are suitable for measurements to be made in aging tests for the purpose of array-lifetime prediction. The need for improved measurements of rates of degradation was identified in a preceding study, also conducted by Battelle for the Low-Cost (Silicon) Solar Array Project, on the development of a "Methodology for Designing Accelerated Aging Tests for Predicting the Life of Photovoltaic Arrays" (Report No. ERDA/JPL-954328-77/1).

The selection of suitable instruments and techniques for lifetime-prediction testing requires an understanding of (1) observed and projected array degradation/failure modes and their causative/contributing factors, (2) the fundamental degradation mechanisms associated with these failures, and (3) the property changes that may be early precursors of this degradation.

Failure Modes and Factors Affecting
Array Performance and Lifetime

Array degradation/failure modes and array lifetime depend upon the individual and combined effects of array design, materials of construction, processing/fabrication methods, and environmental stress factors. The combined effects of the various degradation reactions that occur within the different materials that make up the array (as a result of exposure to key environmental factors such as heat, ultraviolet radiation, moisture, and wind) are the primary concern of studies directed toward array-lifetime prediction.

Observed and projected failure modes for arrays can, for purposes of organization, be related to changes in the values of the components of the lumped-constant photovoltaic device/array model (i.e , current generator, ideal diode, series resistance, and shunt resistance, as shown in Figure A-1). These changes can, in turn, be related to major degradative changes in specific elements or combinations of elements of the module/array, and ultimately to the microscopic (and, in some cases, macroscopic) chemical and physical changes that are the earliest precursors to degradation and failure. Key factors (see Figures A-2 through A-5) are optical losses (e.g., due to discoloration or delamination) that are reflected in the light-generated current, corrosive attack or fracture of contacts, connections, and interconnects, which affect the series resistance; surface-region and pottant conductance changes that result in shunt resistance effects; and fundamental cell-junction characteristic changes that would result in diode losses. This last type of loss is not expected to be significant in normal terrestrial service.

A-1
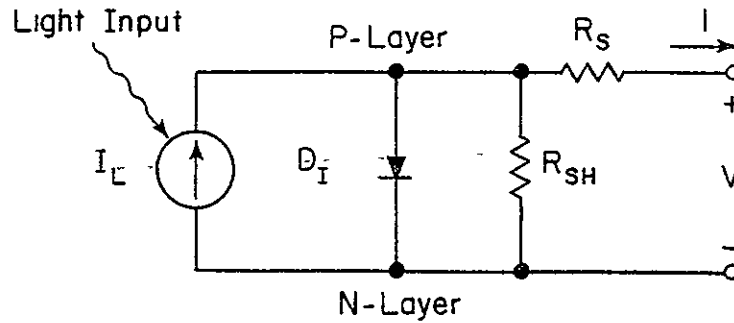
Components of the model
I_L = Light-generated current source
D_I = Ideal diode
R_S = Series resistance
R_{SH} = Shunt resistance

FIGURE A-1. LUMPED-CONSTANT SOLAR CELL MODEL

POWER OUTPUT BELOW SPECIFICATIONS

Series Resistance Increase	Shunt Resistance Reduction	Diode Loss	Light-Generated Current Loss
Gnd Contact Debonding	Pottant Conduction	Junction Alteration	Optical Transmission Losses
Lead Contact Debonding	Surface-State Conduction		Recombination Losses
Lead Fracture	Junction Damage		Cell Fragmentation
Back Contact Debonding			
Gnd Erosion/Corrosion			
Back Contact Erosion/Corrosion			
Surface Layer Resistance Change			
Bulk Si Resistivity Increase			

FIGURE A-2. FOUR FAILURE TYPES BASED ON THE FOUR COMPONENTS OF THE LUMPED-CONSTANT CELL MODEL (FIGURE 1) AND A FIRST-LEVEL BREAKDOWN INTO CAUSATIVE DEGRADATION FACTORS

REDUCTION IN LIGHT-GENERATED CURRENT
DUE TO OPTICAL LOSSES

Reflection	Absorption	Transmissive Scattering	Other
Bulk/Surface Index (n) Change	Surface Absorption	Surface Texture	Mechanical Orientation
No. of Surfaces (Delamination)	Bulk Absorption	Surface Particles (Dirt)	
Surface Texture Change	Surface Particles	Bulk Scattering Centers	
Surface Particles (Dirt)		Interface Scattering	
Optical Coating Thickness Change			

FIGURE A-3. BREAKDOWN OF DEGRADATION FACTORS CONTRIBUTING
TO OPTICAL LOSSES WHICH CAUSE A DECREASE IN THE
LIGHT-GENERATED CURRENT

SERIES RESISTANCE INCREASE

Contact/Connection Debonding	Contact/Interconnect Erosion/Corrosion	Interconnect Fracture	Surface-Layer Sheet Resistance Increase	Bulk Si Resistivity Increase
Chemical Attack Thermal/Mechanical Stress	Chemical Attack	Mechanical Stress	Chemical Erosion Impurity/Dopant Change	Impurity/Defect Changes
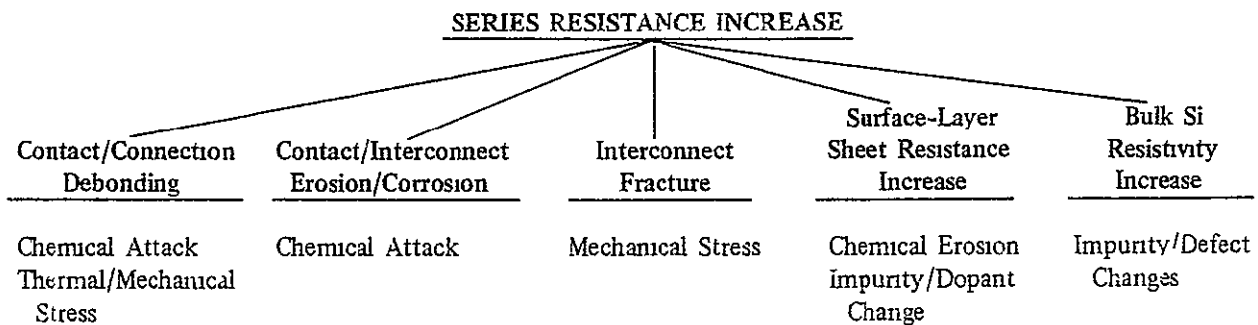
FIGURE A-4. DEGRADATIVE CHANGES MANIFEST AS
SERIES RESISTANCE INCREASES

SHUNTING LOSSES

Junction Damage	Pottant Conduction	Surface Conduction
Chemical Attack	Electrical Breakdown	Surface State/Channel Increase
Mechanical Damage	Chemical Change	
	H_2O Absorption	
	Ionic Accumulation	
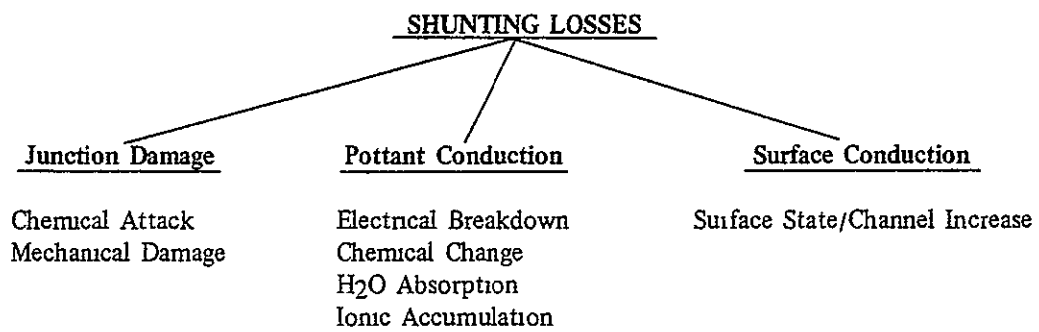
FIGURE A-5. DEGRADATION FACTORS CONTRIBUTING TO LOSSES BY
SHUNT RESISTANCE DECREASES

Microscopic and Macroscopic Property Changes Associated with
Primary Mechanisms of Degradation that Lead to Failure

The early identification of environmentally induced molecular alterations and other minute property changes that can be clearly correlated with observed degradation rates and failure modes is an important and difficult task in the development of a methodology for projecting the operational lifetimes of encapsulated photovoltaic modules/arrays. A major factor contributing to the difficulty of the task is the large number of potential variables (e.g., the large number of candidate materials, materials combinations, and structural designs, as well as the range of environmental conditions that might be experienced). A second, and more fundamental, factor is the lack of theoretical relationships and/or experimental data on quantitative correlations between observed molecular-level or microscopic changes and observed degradation/failure modes for the majority of materials and materials combinations. A third, and equally fundamental, area of difficulty is the lack of a sound scientific basis for predicting the nature and quantity of the microscopic-level changes that will be produced by specified levels of environmental stresses, particularly in cases where synergistic effects involving several environmental factors are involved (as will certainly be the case in actual operation).

The lack of hard data and the immediacy of the needs of the DOE test and demonstration efforts necessitated that, for purposes of this study, preliminary judgments be made as to which of the possible environmentally induced property changes were the most relevant and sensitive indicators of photovoltaic array/module degradation and failure modes. In this context, the major environmental factors contributing to degradation/failure were considered to be ultraviolet radiation, thermal energy, water, oxygen, mechanical and thermal stress, pollutants, and abrasives. The quantitative link between these environmental factors (including their combinations) and the corresponding degradation *rates* are the ultimate objective of the life-prediction process.

Environmental aging of *polymeric materials* is considered to result primarily from photo-oxidation processes that ultimately cause embrittlement, discoloration, and increased dielectric loss. *Glasses* are susceptible primarily to surface attack involving moisture and pollutants of an acidic or alkaline nature. Both polymers and glasses may be subject to abrasive attack from air-borne or waterborne particulates. Cell *contact metallization* and *electrical interconnects* are subject to attack by various corrosive agents that might penetrate through or evolve from the encapsulating materials. Universal among these are water and oxygen. Mechanical and thermally induced stresses can also contribute to the degradation of the integrity of contact metallization and electrical interconnects. Degradation of the basic cell (exclusive of deposited layers such as the metallization and optical control coatings) is believed to be unlikely because of the attack resistance of silicon and the improbability of experiencing temperatures high enough to affect diffusion profiles or significant indiffusion or redistribution of impurities. Catastrophic failures caused by cell cracking can and do occur. These, however, are generally the result of design inadequacies (e.g., thermal mismatch and the presence of high mechanical stress points at specific points in the module) rather than materials or structure degradation. Other array/module components such as the *substrates, frames,* and *edge seals* are likely to be subjected to corrosion or stress-induced changes that will degrade their ability to protect the cell and other electrically and optically functional constituents from environmental factors.

Potentially useful techniques and instruments for degradation measurements were identified through an extensive literature search and through discussions with knowledgeable technical personnel at Battelle and other industrial research laboratories, government laboratories, universities, and instrument manufacturers. For the purposes of the study, the techniques and instruments were organized into six measurement categories — chemical, electrical, optical, thermal, mechanical, and "other physical". The identified techniques and instruments were then screened and evaluated by Battelle researchers in each of the categories, and across categories, using the criteria given in Table A-1. The resulting recommendations of techniques/instruments made for each of the categories are listed below. (A general listing of the major techniques investigated is given in Table A-2.)

Chemical Measurement Techniques

The recommended chemical measurement techniques/instruments are·

- Fourier transform infrared spectroscopy (FTIR)

- Electron spectroscopy for chemical analysis (ESCA)

- Auger electron spectroscopy (AES)

- Chemiluminescence

- Gel permeation chromatography (GPC)

- Mass spectrometry/gas chromatography combination (MS/GC)

- Surface energetics.

Of these recommended chemical techniques, all but chemiluminescence and surface energy analysis are suitable in their present state of development. The FTIR technique (including Attenuated Total Reflection, ATR) is potentially one of the most powerful tools available for studying degradative changes in polymers at their earliest stages. GPC and the MS/GC combination are also potentially powerful techniques for investigating degradative changes due to chain scission, while ESCA and AES will probably find their major applications in destructive tear-down analyses. More data should be obtained on precision capability for all of the recommended tests.

Electrical Measurement Techniques

The recommended electrical measurement techniques are:

- Cell/module/array current-voltage characteristics,
  including spectral response measurements

- Dielectrometry

- Electrical conductance

- Electrical noise measurements

- Special detectors.

Spectral-response measurements will play a key role in testing of devices and modules involved in aging and degradation studies. In order for illuminated I–V characteristics to play a significant role in the quantitative assessment of degradation processes, periodic characterization of the

TABLE A-1. INSTRUMENT AND TECHNIQUE EVALUATION CRITERIA

Properties Measured

Areas of Applicability (material classes, bulk or surface, environments, etc.)

Measured Property Value Ranges and Sensitivity in Ranges

Accuracy in Ranges

Precision in Ranges

Required Form of Test Specimen

Effect of Measurement on Test Specimen (destructive or nondestructive)

Suitability for In-Situ Measurements

Instrument Cost

Ease of Measurement (equipment and specimen preparation, set-up time, run time, monitoring, etc.)

Cost of Test (power and environmental requirements, operator skill level, etc.)

Instrument Portability (size, power requirements, special environmental or cooling requirements, etc.)

Calibration Requirements and Reproducibility Among Instruments

Availability of Instruments

TABLE A-2. TECHNIQUES, INSTRUMENTS, AND PHENOMENA INVESTIGATED FOR APPLICABILITY TO MEASUREMENTS IN LIFETIME-PREDICTION STUDIES

Chemical

Chromatography
Wet Chemistry
Mass Spectrometer
Emission Spectrometer
EPR
NMR
Mossbauer Effect
Thermal/Vacuum Analytical Techniques
SIMS
Neutron Diffraction
X-Ray Diffraction

Electron Microprobe
IR Techniques (FTIR, etc)
Auger
Chemiluminescence
XPS/ESCA
Fluorescent Probe
Electron Stimulated Desorption Spectroscopy
ISS
LEED
Raman Spectroscopy

Electrical

Dielectrometry
Resistivity
Noise Effects
Dark and Light I-V

Cell Patterning (including passive and active devices)
Electron Tunneling Spectroscopy

Mechanical

Rheology
Bond Strength
Elasticity
Tensile Tests

Impact Tests
Acoustical Effects
Flexural Strength

Optical

Spectroscopy
Microscopy
Haze/Gloss Measurements
Optical Wave Guide Effects
Ellipsometry
Reflectance
Absorptance
Scattering Phenomena

Photoelasticity
Magneto-Optical Effects
Piezo-Optical Effects
Laser Diffraction
SEM
Holography
Optical Multichannel Analysis

Thermal

Thermal Conductivity
Thermal Expansion Coefficient
Heat Capacity

Thermal-Analytical Techniques (DSC, DTA, etc.)

Other Physical Techniques

Water Vapor and Gas Permeability
Profilometry

Photoacoustic Spectroscopy

illumination–source spectral characteristics will be required. The quality of the information currently derived from the diagnosis of I–V characteristics is not adequate for service–life prediction for modules having 20-year lifetimes, the goal of the LSA Project. A study to optimize the sensitivity, precision, and accuracy specifically for life–prediction testing is recommended.

Current (1/f) noise measurements should be evaluated for use in studying contact and interconnect corrosion. Dielectric and electrical conductivity measurements are potentially useful in studying several types of degradation–related changes in materials. The incorporation of special detectors or test patterns in arrays is also recommended for further investigation.

Optical Measurement Techniques

Recommended techniques for optical measurements for possible use in life-prediction studies are.

- Reflectometry
- Ellipsometry
- Holographic interferometry
- Light scattering
- Microscopy
- Spectral transmission.

The suitability of simple reflectance measurements for evaluation of first–surface deterioration needs to be determined experimentally for a variety of candidate first–surface materials. Ellipsometric studies should continue with emphasis on problems involved in detecting delamination and and on materials and structures of primary importance. Holographic interferometry experiments should be considered with the objectives of determining the trade–offs between the area scanned and the overall sensitivity and reliability of the technique, and of determining whether strain-birefringence changes, precursory to delamination, can be detected in this way. Optical measurements performed on complete modules or arrays should be limited to a few simple tests, such as spectral transmitted intensity, possibly at only a few selected wavelengths (including UV). Final array designs will play a key role in determining specific measurement procedures.

Thermal and Mechanical Measurement Techniques

The recommended techniques and instruments in the thermal and mechanical properties categories are

- Differential thermal analysis (DTA)
- Differential scanning calorimetry (DSC)
- Torsion pendulum
- Forced vibration viscoelastometer
- Ultrasonic pulse–echo
- Infrared thermovision.

Since the properties of polymers are in some cases very sensitive to the value of the glass transition temperature (T_g), it will be useful to measure this property by a suitable means. The simplest and most rapid methods for measuring T_g appear to be differential thermal analysis and differential scanning calorimetry. In the absence of any information on the relative accuracies of these two techniques with regard to measurement of T_g, DSC measurements would be preferred since the resulting thermograms can be interpreted quantitatively. Alternative methods for obtaining T_g include dynamic mechanical measurement techniques using instruments such as the torsion pendulum and viscoelastometer. This family of techniques also yields potentially valuable data on the mechanical behavior of the materials. Dynamic mechanical measurements would thus be recommended over DTA or DSC in cases where both types of measurements are available. Since temperature is a more important variable than frequency for dynamic mechanical measurements, any of the techniques may be used, depending upon availability and ease of measurement.

The applicability of infrared thermovision in diagnosing solar cell modules merits further testing. The infrared transmission of the various cover and adhesive materials needs to be examined over the wavelength range to which the instrument is sensitive. Also, evaluations need to be made on the spectral emittance of opaque materials and on the possibility of radiation from these materials being propagated through the cover and adhesive materials. The value of infrared thermovision in detecting defects has already been demonstrated, as evidenced by certain areas of modules being hotter or colder than surrounding regions. It is recommended that further testing should be conducted to establish quantitative relationships, such as apparent temperature differences versus a quantitative measure of the degree of the defect.

The applicability of ultrasonic techniques also requires further testing and evaluation. A theoretical analysis appears necessary in order to interpret the various echo signals that may be received. Some experimental testing will be needed in order to select optimum transducers and locations. It is considered that ultrasonic methods have good potential for applicability in this area, and thus tests should be conducted on encapsulated cells with and without defects in order to establish the potential magnitudes of changes in ultrasonic signals that may be experienced.

Other Physical Measurement Techniques

Other physical measurement techniques recommended are.

- Profilometry
- Photoacoustic spectroscopy (PAS)
- Vapor and gas permeability.

Profilometry, when combined with computer processing of the data, could be a powerful tool for quantitative assessment of changes in surface roughness over large areas, such as those that might occur as a result of abrasive attack of photovoltaic module covers. Photoacoustic spectroscopy offers some potentially unique capabilities in studying optical, thermal, and possibly bonding characteristics of polymers; evaluations should be continued to demonstrate its capabilities in studies of photovoltaic-module materials degradation. Permeability measurements of polymeric materials are important for establishing their barrier properties against potential corrosive agents; they could also be useful in diagnosing chemical and structural changes associated with degradation mechanisms in the polymers. Developmental work and experimental evaluations to demonstrate the capabilities are being conducted in another investigation

Adequate experimental data have not been found for comparatively assessing the precision of techniques with potentially overlapping capabilities. This does not exclude interim selections on the basis of other attributes (e.g , availability, field–use capability) but does preclude the recommendation of a preferred technique for measurement, for example, of changes in some polymer properties.

The problem of determining how accurately one can expect to predict the lifetime of a photovoltaic module/array extends beyond the question of the precision associated with a given measurement technique or instrument. Given that, for example, the glass transition temperature can be measured with a known precision, one is still faced with uncertainties in the values of primary derived quantities such as percentage of crystallinity or molecular weight, or in secondary derived quantities that are more directly relatable to module power–degradation rates (e.g., optical transmission). Comprehensive experimental work will be required to establish these relationships.

Recommendations

Three categories of recommendations are addressed.

Establishment of the Adequacy of Existing (Developed) Techniques

In order to establish the limits of the techniques that are more fully developed for this application, the following recommendations are made:

- A determination of the precision for measured properties should be made for ESCA, FTIR, and the MS/GC combination; also, ESCA and FTIR should be compared for measuring surface carbonyl concentration using the Mandel sensitivity–ratio criterion.

- A major effort should be directed toward establishing quantitative correlations between key measurable properties (e.g., polymer molecular weights and glass transition temperatures) and degradation/failure modes.

- A set of experiments to determine the relative precision of the thermoanalytical and dynamic mechanical techniques for measuring glass transition temperature should be conducted.

- Techniques for measuring the current–voltage characteristics of encapsulated cells/modules should be refined to optimize sensitivity, precision, and accuracy for degradation studies.

Potentially Useful Developmental Techniques

The techniques recommended for development, in addition to surface energetics, photoacoustic spectroscopy, and polymer permeability, which are already under investigation, are:

- Electrical noise measurements, electrical-conductivity measurements (polymers), reflectometry and light-scattering measurements, dielectrometry, chemilu-minescence, and the use of special detectors for in-situ measurements for preliminary experimental evaluations

- Holographic interferometry and infrared thermovision for investigation on a high-risk, high-return basis.

Measurement Needs Not Presently Satisfied

Some additional measurement needs are:

- A technique for in-situ determination of changes in the mechanical strength of encapsulation materials for use in degradation studies

- An adequate means for measuring changes in the breaking strength or static fatigue of glass

- A reliable, reasonably inexpensive method for making in-situ spectro-photometric measurements with high precision and over relatively long time periods.

A summary tabulation of the recommended techniques in each of the property-measurement categories, along with values and comments for key selection criteria and other attributes, are given in Tables A-3 through A-7.

TABLE A-3. RECOMMENDED CHEMICAL TECHNIQUES

Instrument/Technique	Properties Measured-- Applicable Degradation Modes	Sensitivity	Accuracy	Precision	Specimen Form	Effect on Specimen	In-Situ Suitability	Cost	Set up/ Run Time	Availability for test	Comments
Fourier Transform Infrared Spectroscopy including ATR	Surface and bulk carbonylization of polymers	100 ppm range?	<0.1 cm^{-1}	<0.1 cm^{-1**}	Various and as little as 25 nanograms	none	No	$120,000	1/2 to 1 hr per specimen	Yes - BCL	--
ESCA	Surface carbonylization of polymers, Depletion of surface species on glass plate, i.e., Na$^+$. Interface evaluation after teardown analysis.	.01 - .02 atomic fraction	*	*	Small flat sheet	Negligible	No	$200,000	5 t 10 specimens per day	Yes	Depth profiling possible in conjunction with ion sputtering.
Gel Permeation Chromatography	Changes in polymer molecular wt. due to chain scission and crosslinking. Detection of low MW species such as residual monomers, plasticers, etc	*	20% at worst	5-7% for Mn or Mw. 1-2% for Mw/Mn	Powder or sheet Small amount	Destructive	No	*	-	Yes	--
Chemiluminescence	Photon emission from degradative reactions	10^{-15} moles/yr degradation rate	*	*	Sheet 3-in dia. or less	none	Possible with specially built apparatus	$6,000 built from individual components	< 30 min.	Yes - BCL	--
Gas Chromatography/ Mass Spectrometry	Volatile polymeric fragments - Photolytic breakdown of polymers	10 ng/mil	10% at worst	*	Any form, down to 10 mg of material	Destructive ‡	No	$30,000 to $150,000	ea 30 min.	Yes	--
Surface Energy	Surface properties	*	*	*	Sheet	none	Yes	$1,000	5-10 min. per liquid		Currently being evaluated.

* Could not be found.

** Repeatability

‡ Not destructive if used as described in the text

A-13 and A-14

TABLE A-4. RECOMMENDED ELECTRICAL TECHNIQUES

Instrument/ Technique	Properties Measured– Applicable Degradation Modes	Sensitivity	Accuracy	Precision	Specimen Form	Effect on Specimen	In-Situ Suitability	Cost	Setup/ Run Time	Availability for Test	Comments
Illuminated I-V Characteristics	$I_{sc}, P_{max}, V_{oc}, R_s,$ R_{sh}– any output degradation	Potentially high	I_{sc}– $\pm$ 2%	I_{sc}– $\pm$ 1%	cell/module/ array	none	yes	\$3K to >\$50K	Setup–few min., Run–seconds or less	Yes – BCL	See Section IV
Dark I-V Characteristics	R_s, R_{sh}, Diode Parameters–cell/ module power dissipation	Potentially high	$\pm$ 0.03% to $\pm$ 0.1%	Potentially high	cell/module/ array	none	Need light tight cell cover	~\$1K up	Setup–run 5 to 15 min.	Yes	See Section IV
Spectral response	I_L vs λ– optical trans- mission degradation	Potentially high	$\pm$ 5% to $\pm$ 20%	$\pm$ 1% at best	cell/module?/ array?	none	crude with filters possible	––	Run– 5 to 30 min.	Yes – BCL	See Section IV
Electrical noise	Current noise – contact corrosion interconnect cor- rosion	––	$\pm$ 0.5 dB (-40 to + 60 dB)	$\pm$ 1 dB	cell/module?/ array?	none	yes	\$3K to \$15K	Setup– Run–nominal	Yes	Requires experimental evaluation
Conductivity	Electrical con- ductivity– ionic impurities moisture content breakdown	Potentially high	$\pm$ 0.03% to $\pm$ 4.0%	Potentially high	Various, known geometry	None, unless excessive temperature excursion	Could be with special custom design	\$0.3K to \$10K	Setup– Run–min.	Yes	Accuracy varies with magnitude; worse for very low conductivities
Dielectrometry	Permittivity, Loss factor– polar groups moisture ions	––	Temp. $\pm$ 1% C $\pm$ 0.02% loss $\pm$ 1%	Temp. $\pm$ 0.25°C	Various, known geometry	None, unless excessive temperature excursion	Conventional– No. Special designs conceivable.	~\$10K to \$15K	Setup–5 to 10 min. Run–min. to hrs.	Yes – BCL	Requires experimental evaluation
Special detectors	Detector Electrical Properties– presence of alien species	Potentially high	Potentially high	Potentially high	module/array	none	yes	––	Built in to module/array. Normal run time	Could design test	––

A-15 and A-16

TABLE A-5. RECOMMENDED OPTICAL TECHNIQUES

Instrument/Technique	Properties Measured-Applicable Degradation Modes	Sensitivity (OPD detectable)	Accuracy (a)	Precision (a)	Specimen Form	Effect on Specimen	In-Situ Suitability	Cost	Set up/ Run Time	Availability for test	Comments
Reflectometry	Reflectance-1st surface degradation, interface changes	200-500 Å	0.1%	1% (long term)	Reasonably flat	None	Possibly, with lower accuracy, precision, etc.	$5,000	Initial setup and test 1-2 days, other times nominal	Yes-could set up at BCL	Scattering angle, not optical path difference (OPD), used in actual measurement
Ellipsometry	Ellipticity of reflected light-delamination, other changes in optical path	5-10 Å (frequently)	0.01%	0 01%	Reasonably flat, can be relatively large	None	No	$10,000 to $50,000	Setup nominal Measure-a few minutes per point	Currently under investigation	---
Holographic Interferometry	Phase change at points in light path-incipient delamination	50-3000 Å	Variable	low long-term with available instruments	Few restrictions	None	No	$30,000	Few minutes to 1 hour per shot	Yes - BCL	High risk, high payoff technique
Light Scattering	Small angle forward scattering of light-delamination, bubble formation, surface damage	high	high	high	Fairly transparent	None	No	$15,000 to $30,000	Nominal	Yes - BCL	Whether delamination occurs in such a way as to cause scattering is not known
Microscopy	Surface structure-first surface damage	50-100 Å resolution for SEM	--	---	Various	None	Yes, with special mounting	> $60,000 for SEM, others vary considerably	Varies with type	Currently in use	—
Spectral Transmission	Transmitted Light-optical transmission degradation, UV damage	high	high	± 1% - ± 2% over 6 months	Various, transparent	None	Possibly with special arrangements	$5,000 - $25,000 for commercial instruments	Minutes to 1 hour	Yes - BCL	Development of suitable field use setup needed

(a) Precision and accuracy are for the quantity measured and not for any derived quantities.

A-17 and A-18

TABLE A-6. RECOMMENDED THERMAL AND MECHANICAL TECHNIQUES

Instrument/ Technique	Property Measured	Sensitivity	Accuracy	Precision	Form of Specimen	Effect of Measurement on Specimen	Suitable for In-Situ Meas.?	Cost	Set up/Run Time	Availability for test	Comments
Differential thermal analysis	Temperature differential/ due to "heat effects"	0.002 C Temp. difference	± 4.0°C for Tg; ~± 2 0°C for T_{melt}	± 2.5°C for Tg, ~± 1.5°C for T_{melt}	Various forms; 0.1 to 100 mg	May or may not be destructive	No	~$20,000 to $25,000	Set up time nominal; run time 10 min. to 2 hrs.	Yes – BCL	
Differential scanning calorimetry	Differential heat input	3 μcal/sec.	± 0.2% on Q ~± 1°C on T	± 1% on Q	Various forms; 0.1 to 100 mg	May or may not be destructive	No	~$20,000	Set up time nominal; run time 10 min. to 2 hrs.	Yes – BCL	
Torsion Pendulum	Dynamic modulus and damping (G' and G")	*	± 4.0°C for Tg; ± 2 0°C for T_{melt} G' for T<Tg, 7% G' for T~Tg, 30% G" for T>Tg 20% G" for T<Tg 10% ± 3 0°C for Tg	± 2.5°C for Tg; ± 1.5°C for T_{melt} G' for T<Tg, 3.5% G' for T~Tg; 15% G" for T>Tg 10% G" for T<Tg; 5%	Rectangular 0.015-0 10 in. by 0 10-0.60 in., 1 to 6 in. long or circular 0 30 in radius, 1 to 6 in. long	Nondestructive	No	~$40,000 for automated system	10 min. to few hrs.	Yes – BCL	
Forced vibration Viscoelast-ometer	Dynamic modulus and damping	*	5-10%	3%	Solid bar 2mm x 2mm x 2cm	Nondestructive	No	$25,000 to $50,000	Set up:15 min. to few hr. Run time:1 hr for several frequencies at a given temperature	Yes-BCL(Weissenberg Rheogoniometer)	
Ultrasonic Pulse-echo	Flow detection	*	*	*	--	Nondestructive	Yes	~$ 5,000	Several minutes	Yes – BCL	Needs further theoretical and experimental evaluation; currently under investigation.
Infrared Thermo-vision	Temperature differences at flaws	0.2°C	*	*	--	No effect	Yes	~$45,000	Several minutes	Yes – BCL	Needs further evaluation to account for non-blackbody radiation and transparency in sensitive wavelength range.

A-19 and A-20

TABLE A-7. OTHER RECOMMENDED TECHNIQUES

Instrument/Technique	Properties Measured-Applicable Degradation Modes	Sensitivity	Accuracy	Precision	Specimen Form	Effect on Specimen	In-Situ Suitability	Cost	Set up/ Run Time	Availability for test	Comments
Profilometry	Surface roughness - surface etch/leach abrasion	CLA $\pm$ 2% (2-400 μ in.) H$\pm$ 1 to 200 μin. (20-4000 μ in.)	--	$\pm$ 2%	Flat or circular curvature	0.1 gm force on 1-10μ radius tip	Conventional is lab only; special design conceivable	$10K +	Tedius adjustment/ 0.2 - 180 gm/min	Yes - BCL	Roughness sensitivity of 5 Å claimed for Dektak unit coupled with computer.
Water Vapor & Gas Permeability	Flow rate of Gas/ WV through material-molecular wt, crystallinity cross linking, density	WVTR-0.01 gm/100 in.^{2}/24 hr	Temp. $\pm$ 0.5°F WVTR- $\pm$ 2%	$\pm$ 10%	Generally sheet	none	Conventional no	$1K - $14K	~1 hr/ 30 min to days	Currently under investigation	none
Photoacoustic Spectroscopy	Optical Absorption, Thermal Diffusion-optical properties	11 mV/mW	*	*	Various	none	no	$25K - $30K	-	Currently under investigation	none

A-21 and A-22